Biometals
https://doi.org/10.1007/s10534-022-00418-0

Property evaluation of two anticancer candidate platinum complexes with *N*-isobutyl glycine ligand against human colon cancer

Zahra Hosseini-Hashemi · Masoud Mirzaei · Mahboube Eslami Moghadam

Received: 21 December 2021 / Accepted: 27 June 2022

Abstract Small molecules have potential usage in cancer therapy due to their remarkable potency of disarranging the natural structure of nucleic acids. In this study, two complexes $[Pt(NH_3)_2(IBgly)]NO_3$ (**1**) and $[Pt(bipy)(IBgly)]NO_3$ (**2**) based on Pt(II), *N*-isobutylglycine (IBgly), 2,2′-bipyridine, and ammonia were prepared and characterized by spectroscopic methods. Pharmacokinetic ADME data, absorption, distribution, metabolism, excretion, and bioavailability radar showed two complexes can be introduced for Pt-based anti-cancer drugs. Mechanism of tumor inhibition and DNA interaction of these compounds was studied by UV–Vis, fluorescence, and CD spectroscopies. Also, thermodynamic parameters and the binding constants were calculated through absorption measurements. The fluorescence data showed that a static quenching mechanism occurred for both complexes with a binding constant and binding affinity towards DNA ($K_b \approx 3500$ M^{-1} and $k_q \approx 2.1 \times 10^{11}$ M^{-1} s^{-1}). The thermodynamic parameters indicated electrostatic approaching and groove binding were more feasible than intercalation mode between Pt(II) complexes and DNA. CD spectra indicated the increasing intensity of the positive band and the negative band decreasing. Density functional theory calculations confirmed the experimental data and determined the quantum chemical descriptors including total energy, hardness, chemical potential, electrophilicity, electronegativity, etc. According to this, the binding tendency of these compounds with DNA could be predicted. Further, molecular docking studies were also performed. Docking studies revealed that the desolvation, hydrogen, and electrostatic binding were effective for the interaction between complexes and DNA with binding energy (−10.44 and −9.57 kcal/mol) for complexes **1** and **2**, respectively, which is mainly of partially electrostatic and groove binding type. The cytotoxic activity of Pt complexes was examined against human colon cancer cell line which indicated good activity with IC_{50} values of (41.66 and 47.30 μM) for both complexes after 72 h, respectively. Also, they demonstrated more inhibitory effects compared to carboplatin.

In memory of our colleague, mentor, and friend, Professor Hossein Eshtiagh-Hosseini (1947–2021) whose friendship will always remain in our hearts and his advice forever in our minds.

Supplementary Information The online version contains supplementary material available at https://doi.org/10.1007/s10534-022-00418-0.

Z. Hosseini-Hashemi · M. Mirzaei (✉)
Department of Chemistry, Faculty of Science, Ferdowsi University of Mashhad, Mashhad, Iran
e-mail: mirzaeesh@um.ac.ir; mirzaei487@yahoo.com

M. Eslami Moghadam (✉)
Chemistry & Chemical Engineering Research Center of Iran, Tehran, Iran
e-mail: eslami_moghadam@ccerci.ac.ir; eslami_moghadam@yahoo.com

Published online: 13 July 2022

Graphical abstract

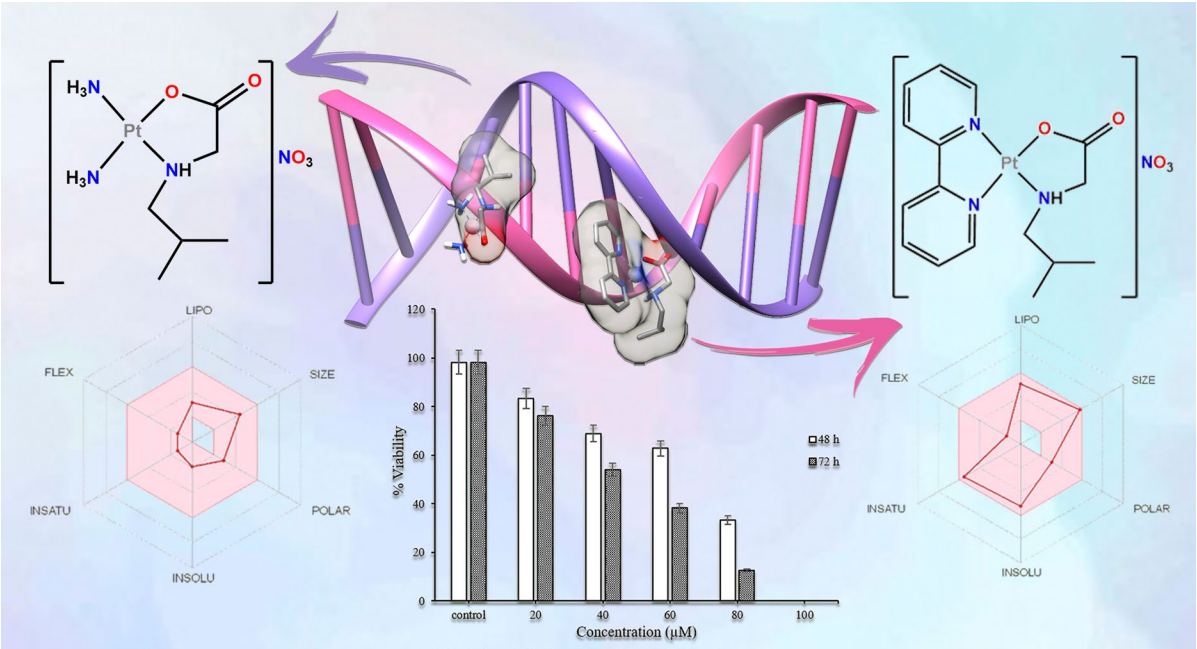

Keywords Pt(II) complexes · *N*-isobutylglycine · DNA-binding studies · DFT · Molecular docking · Cytotoxic activity

Abbreviations

ADME	Absorption, distribution, metabolism, and excretion
BBB	Blood–brain barrier
bipy	2,2′-Bipyridine
CT-DNA	Calf thymus DNA
EB	Ethidium bromide
CD	Circular dichroism
DFT	Density functional theory
FMOs	Frontier molecular orbitals
IBgly	*N*-Isobutylglycine
K	Equilibrium constant
K_b	Binding constant
k_q	Biomolecular quenching constant
K_{sv}	Stern–Volmer quenching constant
MEP	Molecular electrostatic potential
NBO	Natural bond order
QCDs	Quantum chemical descriptors
PGP	P-glycoprotein
PDB	Protein data bank
Tris-buffer	Tris(hydroxymethyl)aminomethane hydrochloride

Introduction

International Agency for Research on Cancer (IARC) has reported about eighteen million new cancer instances which about ten million cancer deaths have occurred worldwide in 2018 (Bray et al. 2018). There are several ways available for cancer therapy including surgery, chemotherapy, immunotherapy, radiation therapy, hormone, and gene therapy, as well as stem cell transplantation. Among them, the most common method is chemotherapy, especially if cancer has progressed or is malignant (Zhao et al. 2018; Fan et al. 2017). Cisplatin, the first FDA-approved chemotherapy drug based on metal complexes, impairs transcription and synthesis of DNA. It is mostly used in the inhibition of ovarian, testicular, cervical, and

other cancers (Zhao et al. 2018; Hoffman et al. 2016; Rozencweig et al. 1977; Raudenska et al. 2019; Wiltshaw 1979). Nevertheless, side effects such as vomiting, nephrotoxicity, ototoxicity, and gastrointestinal toxicity have prompted pharmacologists and bioinorganic chemists to design and synthesize new metal-based therapeutics (Oun et al. 2018; Liu et al. 2019). Modification of chloride ligands of cisplatin, as leaving groups, protects and prohibits biodegradation of cisplatin compound before it reaches the target cells. This strategy can probably mitigate the side effects and disadvantages (Wilson and Lippard 2014). Selecting simple biomolecules would be a proper solution due to biological compatibility with the human body, easier drug transfer, and less toxic effects after drug decomposition. Amino acids such as glycine with both carboxyl (–COOH) and amino ($–NH_2$) groups and the general formula ($NH_2CHRCOOH$) are good candidates that can coordinate with platinum forming a stable five-membered chelate ring through N- and O-bidentate chelating mode (Iakovidis and Hadjiladis 1994; Mansouri-Torshizi et al. 2019; Imaz et al. 2011). Following the previous works of our research team, we attached an aliphatic branch (*N*-isobutyl) to glycine and synthesized its Pt(II) complexes is according to above mentioned, several Pt and Pd complexes based on derivatives of amino acid glycine have been synthesized and their anticancer properties have been investigated (Farhangian et al. 2017; Eslami Moghadam et al. 2016; Ghalandari et al. 2019). For this purpose, an aliphatic derivative of glycine (*N*-isobutylglycine) and two platinum complexes, $[Pt(NH_3)_2(IBgly)]NO_3$ (**1**) and $[Pt(bipy)(IBgly)]NO_3$ (**2**), were chosen to investigate lipophilicity, solubility and anticancer activities (Ramezani et al. 2021a, b; Safa Shams Abyaneh et al. 2018) and synthesized and characterized by some physicochemical analyses. Several physicochemical and pharmacokinetic properties of these candidates' anticancer Pt-drugs were predicted and investigated by ADME. The theoretical studies (density functional theory (DFT) and molecular docking) of Pt(II) complexes were performed. The interaction of these compounds with CT-DNA was performed by electronic absorption spectroscopy (UV–Vis), fluorescence, and circular dichroism spectroscopies. The cytotoxic effects of these compounds were explored for in vitro cytotoxic activity against human colon cancer cell line HCT116 cell lines and compared with cisplatin using an MTT assay.

Experimental

Materials and methods

All chemicals, solvents, and highly polymerized calf thymus DNA were prepared from Merck (Germany), Riedel, and Sigma-Aldrich. Solvent purification was done before using them. The *cis*-$[Pt(NH_3)_2I_2]$ and $[Pt(bipy)Cl_2]$ were prepared and purified according to the literature procedures (Drew et al. 1932; Cohen and Lippard 2001; Liang et al. 2015; Miskowski et al. 1993). Infrared spectra (4000–400 cm^{-1}) were recorded in KBr disks on a JASCO-460 plus FT-IR spectrophotometer. The mass spectrum was scanned on an MS model CH7A Varian (EI, 70 eV). On a Shimadzu LCMS-2010 A, liquid chromatography-mass spectrometry (LC–MS) studies and a Netzsch-TGA 209 F1, thermal gravimetry analysis were performed. ^{1}H NMR, ^{13}C NMR, ^{195}Pt NMR spectra were recorded by Brucker BRX-250 Avance spectrometer at 300, 75, and 64 MHz, respectively with DMSO-*d*6 as a solvent. The conductivity of two complexes was carried out on a Systronics Conductivity Bridge, model 305, with a cell constant of 0.59 using water as the solvent. Melting points were recorded by, a Buchi B-545. SPEKOL 2000 UV 6800 recording spectrophotometer was used for absorbance reported. The fluorescence emissions were determined by a Hitachi MPF-4 spectrofluorimeter. Finally, circular dichroism was measured using a Jasco J-1500 CD spectrometer. Abbreviation of multiplicities are shows: s = singlet, d = doublet, t = triplet, br = broad, m = multiplet.

Synthesis of ligand and metal complexes

Synthesis of N-isobutylglycine

N-isobutylglycine (IBgly) was synthesized by modifying the method reported in the literature (Fugger et al. 1955). Generally, a solution of ethyl bromoacetate (10.6 mmol, 1.20 mL) in toluene (2 mL) was added dropwise with constant stirring to a solution of Isobuthylamine (21.2 mmol, 2.16 mL) in toluene (8 mL) in an ice bath and stirred for 30 min. After refluxing for 4 h and cooling, the Isobutylamine hydrobromide was filtered off, washed with toluene, and dried. The filtrate was concentrated until the entire toluene as a solvent was removed by a rotary evaporator under reduced pressure. Sodium hydroxide

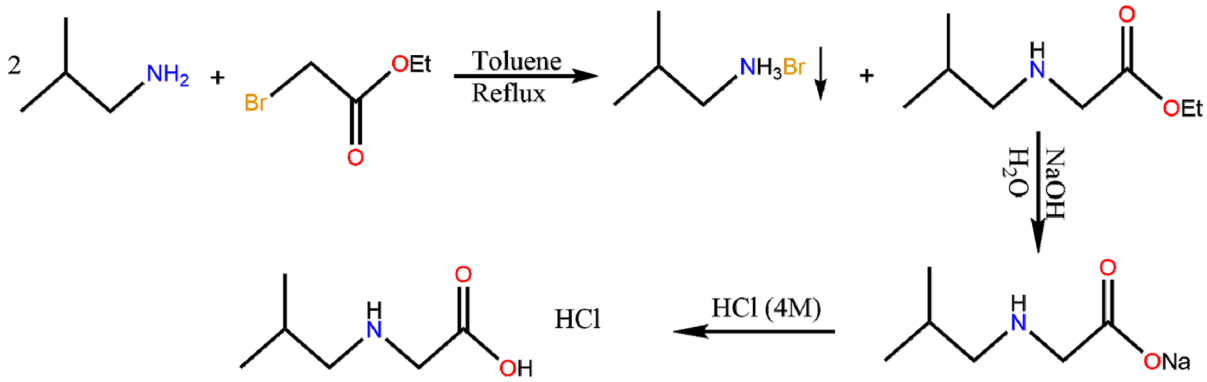

Scheme 1 Preparation routes of IBgly

(10.6 mmol, 0.42 g) dissolved in 1.6 mL distilled water was added to the above-concentrated solution and refluxed for 30 min and then cooled. The solution and diethyl ether (10 mL) was poured into a separatory funnel with the mixture extracted three times with (10 mL) diethyl ether to remove primary organic materials and solvent. The aqueous solution was acidified with HCl (3 mL, 4 M) until the pH reached 2.0. Finally, a yellow precipitate was obtained with slow evaporation at 35 °C. This ligand was purified through recrystallization from a minimum amount of HCl 0.1 M (see Scheme 1).

IBgly·HCl (*N*-isobutylglycine·HCl): Yield: 65% with a melting point of 212–215 ℃. Analytical calculated for $C_6H_{14}ClNO_2$ (167.07 g mol^{-1}): C, 42.99; H, 8.42; N, 8.36. Analytical found: C, 42.54; H, 8.01; N, 7.98%; IR bands (KBr pellet, cm^{-1}): 3500(br), 2955(br), 2592(w), 2385(m), 1761(s), 1468(m), 1418(s), 1218(s), 905–799(m). ^{1}H NMR (300 MHz, DMSO-d_6, 323 K, TMS): δ 0.92 (d, $^3J_{H-H}$ = 6.69 Hz, 6H), 2.00 (m, $^3J_{H-H}$ = 6.77 Hz, 1H), 2.75 (d, $^3J_{H-H}$ = 7.05 Hz, 2H), 3.79 (s, 2H), 9.14 (sb, NH), 13.15 (sb, OH). ^{13}C{1H} NMR (75 MHz, DMSO-d_6, 333 K, TMS): δ 20.08 (s, 2C), 25.29 (s, 1C), 47.26 (s, 1C), 53.96 (s, 1C), 167.87 (s, 1C=O). MS (70 eV, EI): m/z (%) = 131 (5) $[M]^+$, 130 (25) $[M-H]^+$, 87 (87.5) $[M-COOH]^+$, 59 (82) $[M-C_4H_{11}N]^+$, 56 (63) $[C_4H_8]^+$, 45 (35) $[COOH]^+$, 41 (100) $[C_2H_3N]^+$, 30 (83) $[CH_2NH_2]^+$. The MS, ^{1}H NMR, and ^{13}C NMR spectra of IBgly are given in Figures S1-S3 in supplementary information.

Synthesis of Pt(II) complexes

Synthesis of $[Pt(NH_3)_2(IBgly)]NO_3$ (1)

$AgNO_3$ (0.11 g, 0.63 mmol) was dissolved in double-distilled water (43 mL) and then *cis*-$[Pt(NH_3)_2I_2]$ (0.15 g, 0.31 mmol) was added slowly while stirring. The suspension was heated while stirring at 40 °C for 24 h under darkness and Argon gas atmosphere. After the reaction was completed, the mixture was filtered

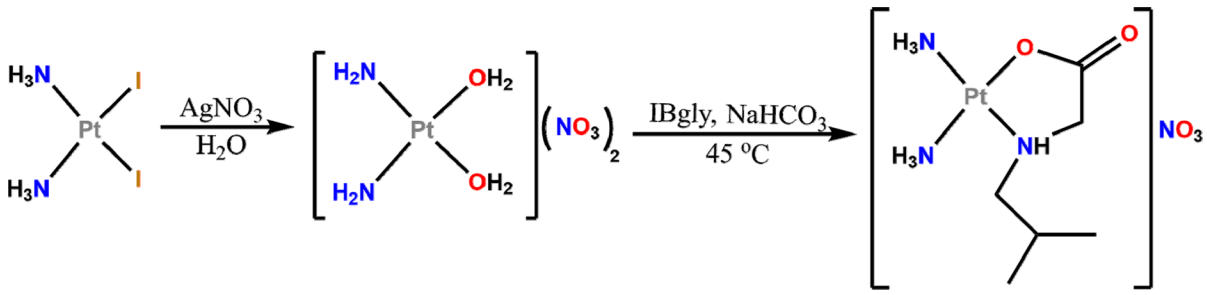

Scheme 2 Preparation route of complex **1**

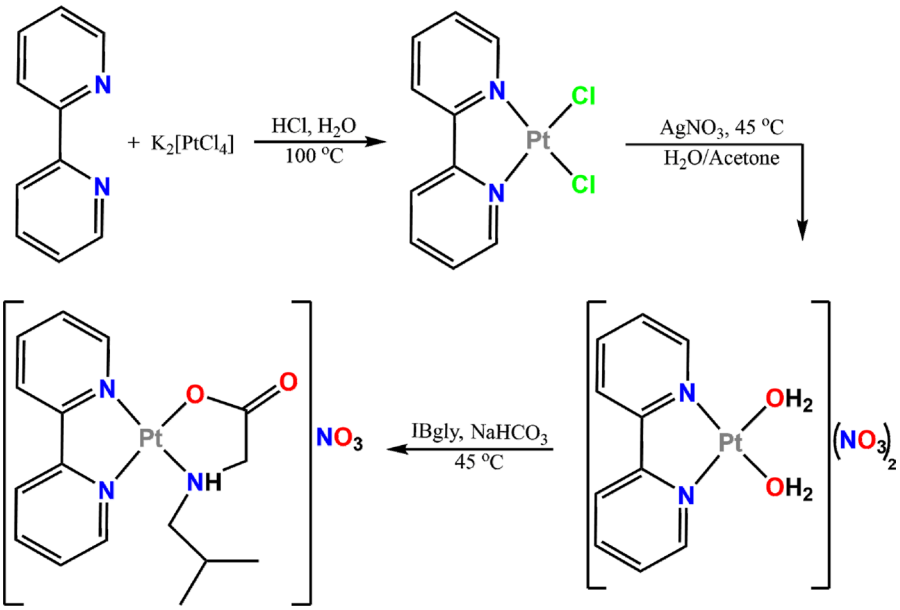

Scheme 3 Preparation route of complex **2**

through Whatman 42 filter paper to remove the AgI precipitate. In a separate beaker, IBgly (0.08 g, 0.38 mmol) and $NaHCO_3$ (0.06 g, 0.69 mmol) were dissolved in double-distilled water (20 mL) at 45 °C with constant stirring and added dropwise to filtrate under darkness and concentrated at 35 ℃. The yellow precipitate of **1** was obtained and washed with some water and acetone. Then, it was kept in a vacuum desiccator to dry. Due to purification, complex **1** was recrystallized with a minimum amount of double distilled water twice (see Scheme 2).

$[Pt(NH_3)_2(IBgly)]NO_3$: The yield of the reaction was 71% with a decomposing temperature of 208 °C. Analytical calculated for $C_6H_{18}N_4O_5Pt$ compound (421.32 g mol^{-1}) is C, 17.10; H, 4.31; N, 13.30%. Analytical found: C, 17.45; H, 4.77; N, 12.89%; IR bands (KBr pellet, cm^{-1}): 3440(br), 3197(br), 2869(m), 1644(s), 1383(s), 1170(w), 1049(w), 834(m), 701(w), 541(w), 461 (w); UV Band λ_{max} (nm) ε_{mM} ($Lmmol^{-1}$ cm^{-1}): 209 (68.26); Molar conductance, ΛM (10^{-4} M, H_2O) = 132 Ω^{-1} cm^2 mol^{-1}; ^1H NMR (300 MHz, DMSO-d_6, 323 K, TMS): δ 0.90 (m, 6H), 1.94 (m, 1H), 2.07, 2.56 (s, m $^3J_{H-H}$ = 188.44 Hz, 2H), 2.63, 3.12 (d, s, $^3J_{H-H}$ = 144.49 Hz, 2H), 3.41 (m, NH_3), 4.44 (m, NH_3), 6.24 (s, NH); $^{13}C\{1H\}$ NMR (125 MHz, DMSO-d_6, 298 K, TMS): δ 20.54 (s, 2C), 27.09 (s, 1C), 52.05 (s, 1C), 56.22 (s, 1C), 174.37 (s, 1C = O). ^{195}Pt-{^1H} (64 MHz, DMSO-d_6, 300 K, TMS): δ −2966.21 ppm. $[M]^+$–NO_3: 358.90; The ^1H NMR, $^{13}C\{1H\}$ NMR, ^{195}Pt-{^1H} NMR, and LC-Mass spectra of complex **1** are given in Figs. S4–S7 in supplementary information.

Synthesis of [Pt(bipy)Cl_2]

$[Pt(bipy)Cl_2]$ was prepared and purified according to the literature procedure (Liang et al. 2015; Miskowski et al. 1993).

$[Pt(bipy)Cl_2]$: Yield: 95%. ^1H NMR (300 MHz, DMSO-*d*6, 323 K, TMS): δ 8.15 (dd, $^3J_{H-H}$ = 5.49, 13.69 Hz, 2H), 8.27 (s, 2H), 9.02 (d, $^3J_{H-H}$ = 8.21 Hz, 2H), 9.67 (d, $^3J_{H-H}$ = 5.29 Hz, 2H). The ^1H NMR spectrum of $[Pt(bipy)Cl_2]$ is given in Figure S8. in supplementary information.

Synthesis of [Pt(bipy)(IBgly)]NO_3 (2)

A suspension of $[Pt(bipy)Cl_2]$ (0.14 g, 0.33 mmol) and $AgNO_3$ (0.11 g, 0.66 mmol) was placed in a round-bottom flask in double-distilled water–acetone (1:3; 178 mL) under Argon gas atmosphere and dark conditions at 45 °C untile the green precipitate of AgCl appeared. The precipitate was eliminated by filtering through Whatman 42 filter paper. A solution of IBgly (0.08 g, 0.40 mmol) and $NaHCO_3$ (0.06 g, 0.73 mmol) in 30 mL double distilled water was added dropwise to clear yellow filtrate under darkness

at 45 °C. The yellow product of **2** was obtained and washed with double distilled water plus acetone through evaporation of solution at 35 °C. Complex **2** was recrystallized with double distilled water twice (see Scheme 3).

[Pt(bipy)(IBgly)]NO_3: The yield of the reaction was 71% with a decomposing temperature of 293 °C. Analytical calculated for $C_{16}H_{20}N_4O_5Pt$ compound (543.44 $gmol^{-1}$) is C, 35.36; H, 3.71; N, 10.31%; Analytical found: C, 35.63; H, 3.78; N, 10.27%; IR bands (KBr pellet, cm^{-1}): 3439(br), 3089(m), 2889(m), 1686(s), 1384(s), 1204(w), 1040(m), 816(m), 732(w), 519(w), 465 (w); UV Band maxima in nm (ε_{mM} in $Lmmol^{-1}$ cm^{-1}): 246 (21.36), 294(6.068), 305(10.97), 317(15.98), 342(2.37); Molar conductance, ΛM (10^{-4} M, H_2O) = 129 Ω^{-1} cm^2 mol^{-1}; ^{1}H NMR (300 MHz, DMSO-d_6, 323 K, TMS): δ 1.04 (d, d, $^3J_{H-H}$ = 6.66 Hz, 6H), 2.13 (m, 1H), 2.93 (m, 2H), 3.57(d, $^3J_{H-H}$ = 16.54 Hz,1H), 3.92 (d, $^3J_{H-H}$ = 15.00 Hz,1H), 7.46 (s, NH), Aromatic protons: 7.91(q, $^3J_{H-H}$ = 6.08 Hz, 2H), 8.48(m, 2H), 8.66(m, 3H), 8.75(d, $^3J_{H-H}$ = 6.00 Hz,1H); ^{13}C{1H} NMR (75 MHz, DMSO-d_6, 300.0 K, TMS): δ 20.29 (s, 1C), 20.79 (s, 1C), 25.40 (s, 1C), 54.28 (s, 1C), 63.06 (s, 1C), 124.31 (s, 1C), 124.67 (s, 1C), 128.15 (s, 1C), 128.40 (s, 1C), 141.37 (s, 1C), 141.94 (s, 1C), 148.59 (s, 1C), 150.39(s, 1C), 155.60 (s, 1C), 156.50 (s, 1C), 180.50 (s, 1C); ^{195}Pt-{^{1}H} (64 MHz, DMSO-d_6, 300 K, TMS): δ-2970.86 ppm. $[M]^+$–NO_3: 480.75; The ^{1}H NMR, ^{13}C NMR, ^{195}Pt-{^{1}H} NMR, and LC-Mass spectra of complex **2** are given in Figures S9-S12 in supplementary information.

ADME prediction

One of the most essential parts of drug discovery and drug molecule development is the prediction of ADME parameters before experimental research (http://www.swissadme.ch). ADME studies have always been crucial in assisting the optimization of new medication pharmacokinetic features, hence boosting their success rate. Lipinski's rule of five analysis was used to determine whether a chemical compound might be used as an orally active medicine in humans (Daina et al. 2017; Ramya et al. 2018).

Theoretical calculation

All geometric optimizations and energy calculations of IBgly, as well as complexes **1** and **2**, were carried out using density functional theory (DFT) at the UB3LYP and 6-311G basis set for H, C, N, and O atoms and (LANL2DZ) were utilized for Pt metal atom using Gaussian 09 program. The input file of IBgly and Pt-derivatives was obtained using GausView 6.0 program (Frisch et al. 2009; Dennington et al. 2016). Also, the electrostatic potential (ESP) charges were determined to obtain the molecular electrostatic potential (MEP) maps for electron delocalization determining in the molecular surface. Further, some quantum chemical parameters were computed in the aqueous phase (Pearson 1986; Imram et al. 2019). They are the energy of the lowest unoccupied molecular orbital (E_{LUMO}), the energy of the highest occupied molecular orbital (E_{HOMO}), the energy gap between LUMO and HOMO ($E_{GAP} = E_{LUMO} - E_{HOMO}$), ionization energy ($I = -E_{HOMO}$), electron affinity ($A = -E_{LUMO}$), absolute hardness [$\eta = -1/2(E_{LUMO} - E_{HOMO})$], absolute softness ($\sigma = 1/\eta$), absolute electronegativity ($\chi = -1/2(E_{LUMO} + E_{HOMO})$), chemical potential ($CP = -\chi$), global softness ($S = 1/2\eta$), electrophilicity index ($\omega = CP^2/2\eta$), nucleophilicity index [$N = (1/\omega)$], and additional electronic charges [$\Delta N_{max} = -(CP/\eta)$].

Docking simulation study

The receptor structure [1BNA: 5′-D(*CP*GP*CP*GP*AP*AP*TP*TP*CP*GP*CP*G)-3′] was downloaded from the Protein Data Bank (http://www.rcsb.org/pdb). Docking simulation of Pt complexes-DNA interaction was studied using AutoDockTools 1.5.6 with AutoGrid 4.2.5 and AutoDock 4.2 [AutoDock 4.2 Release 4.2.5.1(c) 1989–2012] (Morris et al. 2019). The structure of the complexes was optimized using Gauss View 6.0 program and optimized by the theoretical level of UB3LYP with 6–311 G basis set for (H, C, N, and O) atoms, along with LANL2DZ basis set for platinum metal with the Gaussian 09 program. All water molecules as solvent were removed before docking after which the charges, Gasteiger partial charges, and hydrogen atoms were added to the receptor. The grid dimensions were kept 84 × 104 × 126 and 86 × 112 × 122 Å points in x, y, z directions for complexes **1** and **2**, respectively, and

a grid-point spacing of 0.375 Å. The search for best conformers was done using the Lamarckian Genetic Algorithm (LGA). Finally, the molecular docking figures were obtained using the AutoDock program.

Experimental DNA interaction with Pt-complex

The spectroscopic isothermal titration, 50 µL of 1 mM solution of Pt(II) complexes **1** and **2,** (stock solution: 1 and 0.5 mM, respectively) were separately titrated in 1.8 ml of Tris–HCl buffer (10 mM sodium chloride, pH 7.4) and CT-DNA solution (0.08 mM). Buffer solution without CT-DNA and Pt complex was used as reference. An equal amount of the metal complex solution was added to the reference solution to eliminate the absorbance of each complex. After 1 min., the absorbance was recorded at 258 and 640 nm. Absorbance at 640 nm was used to eliminate the interference of solutions turbidity. Upon no changes were observed in absorbance, titration was stopped and absorbances were plotted against different concentrations of each complex. This experiment was separately performed at 27 and 37 °C (Xu et al. 2008). To state the denaturation mechanism, the thermodynamic and binding parameters were mainly obtained via the PACE method (Greene and Pace 1974).

The thermal denaturation was carried out in phosphate buffer through continuous heating from 25 to 99 °C each 2 °C/min. The electronic absorbance variations were monitored at 258 nm. The temperature at the midpoint of the transition denaturation of DNA is the melting point (T_m) and is distinguished as the temperature at which half of the DNA double helix changes into a single strand (Lehninger et al. 2005; Hosseinzadeh et al. 2020).

Fluorescence emission of ethidium bromide was applied in water because it shows feeble fluorescent as a fluorescent probe to double-stranded via intercalation between base pairs of DNA (Wani et al. 2020; Lakowicz 2006; Albani 2007). The fluorescence emission spectra were considered at 471 nm and registered from 540 to 700 nm (slit width was 10 nm) representing fluorescence maxima at 580 nm. Recorded fluorescence emission of Pt complexes was according to baseline during monitoring. The solution of 12×10^{-2} mM DNA and 2×10^{-3} mM EB was titrated by 0–0.31 and 0–0.20 mM of **1** and **2**, respectively, at room temperature.

In circular dichroism as an optical technique, the intercalation bond enhances the absorption of the first band in the CD spectrum due to the π–π* interaction. Base stacking (275 nm) yields the positive band, whereas right-handed helicity causes the negative band (245 nm) (Rehman et al. 2015a, b). The ellipticities of DNA changed conformational structure at 0.12 mM in the range of 200–320 nm at 25 °C by adding each complex of **1** and **2** in the range of (0.2–0.43 and 0.05–0.13 mM) for complexes **1** and **2**, respectively.

In vitro Cytotoxicity data

Human colorectal cancer cell line HCT116 was procured from the NCBI Pasteur Institute of Iran. To grow the cells, the DMEM medium (Sigma) was supplemented with 2 mM L-glutamine, 5 µg/mL streptomycin, penicillin, and 10% heat-inactivated fetal calf serum under 5%:95% CO_2: air atmosphere at 37 °C. For assays of the cell proliferation, the soluble yellowish MTT was broken and transformed into the insoluble purple formazan which is activated by mitochondrial dehydrogenase of living cells. According to the MTT assay, the cell viability assay from the cytotoxicity effects of complexes **1** and **2** was studied in a 96-well plate (1×10^4 cell/mL) and overnight adherence. Next, HCT116 cell lines were incubated with different concentrations of Pt(II) complexes to 0–100 µM and incubated for 48 and 72 h. Four hours before completing the incubation, 25 µL of the MTT solution (5 mg/mL in PBS) was appended to the cultured media, after which the insoluble formazan was made. Later, optical density (OD) of the dissolved insoluble formazan produced was read in 10% SDS and 50% DMF solution (left for 2 h at 37 °C in darkness) and optical density (OD) at 570 nm against reagent blank via a multi-well scanning spectrometer (ELISA reader, Model Expert 96, Asys Hitech, Austria).

Results and discussion

Ligand coordination and complex formation

TGA/DTG analysis of two Pt-complexes was detected with a 10 ℃ min^{-1} heating rate under N_2 atmosphere and weight loss were measured from ambient temp.

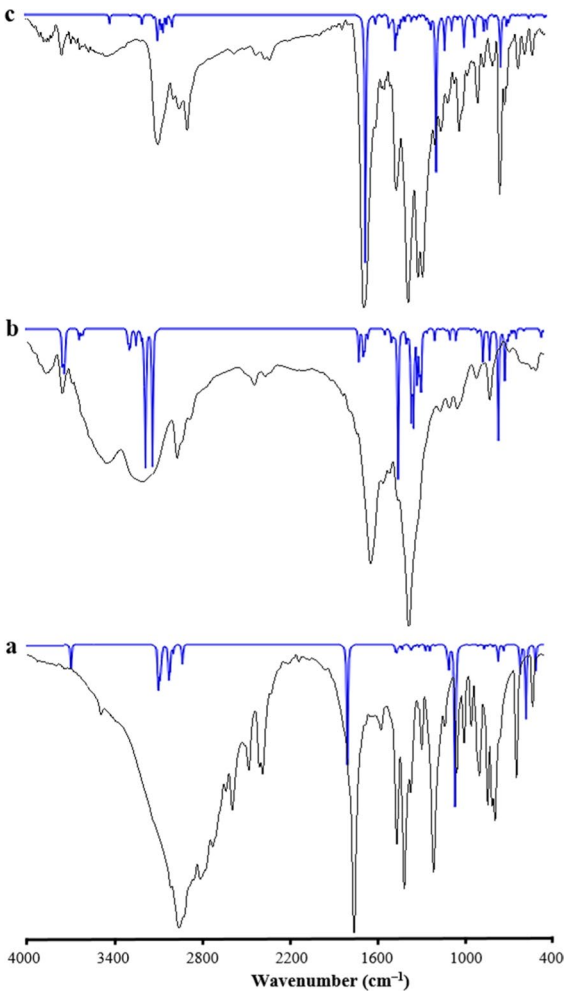

Fig. 1 Experimental IR and FREQ-DFT computational IR spectra of **a** IBgly, **b** and **c** complexes $[Pt(NH_3)_2(IBgly)]NO_3$ (**1**) and $[Pt(bipy)(IBgly)]NO_3$ (**2**), respectively. The computational and experimental IR spectra are shown as blue and black lines, respectively

to 800 ℃. The mass change for **1**: 52.7 and **2**: 39.8% displays PtO and Pt/PtO residue is in ashe at 800 ℃ and presence of ligands is proved by mass change percent determined for two compounds (Fig. S13 in the supplementary information). These numbers of percent are according to mass recorded at mass spectra in Figs. S7 and S12 in the supplementary section. Similar to the KBr pellet IR spectrum of other amino acids, the IBgly is also broad exclusively within the range of 2000–3500 cm^{-1}. The FT-IR spectra of IBgly as free amino acid and its Pt complexes are displayed in Fig. 1. The broad bands arising due to OH stretching vibration can be assigned to the carboxylate group of the IBgly and complexes at 3439–3494 cm^{-1} (Fischer et al. 2005; Nakamoto 2009; Rosado et al. 1998). Assignment of the NH and CH stretching vibrations in the free IBgly and both complexes appeared in the region of 3335–2723, 3197–2869, and 3089–2889 cm^{-1}, respectively. The strong bands around 1761 and 1418 cm^{-1} are attributed to $\nu_{as}(COO^-)$ and $\nu_s(COO^-)$ in IBgly. The redshift of the asymmetric and symmetric stretching vibrations of the carboxylate group in complexes **1** and **2** within the range 1644–1686 and 1383–1384 cm^{-1}, respectively, indicates the fact that the IBgly has been coordinated to the platinum center by the oxygen atom of the carboxylate group. The identification between unidentate or bidentate coordination mode of glycine to platinum is detected by infrared spectra. If the bidentate (chelated) glycino group was absorbed at 1643 cm^{-1}, the ionized or the un-ionized unidentate group would be absorbed at 1610 and 1708 cm^{-1}, respectively. In both complexes, the glycino group appeared at 1644 and 1686 cm^{-1} which can be considered as a bidentate (chelating) group (Nakamoto 2009; Latha et al. 2017; Kieft and Nakamoto 1967). The bands at 1218, 1170, and 1204 cm^{-1} would be attributed to C–N stretching vibrations of IBgly and complexes, respectively. Also, it can be considered respectively for **1** and **2** the weak bands at 1049, 834, and 701 and 1040, 816, and 732 cm^{-1} for the nitrate ion (Castro and Jagodzinski 1991). Ultimately, the ν(Pt–N) and ν(Pt–O) are ascribed at 569–519 and 461–465 cm^{-1} for complexes **1** and **2**, respectively (Nakamoto 2009).

DT-DFT and Freq-DFT computational studies can be used for the validation of all proposed structures. The geometry of each complex has been optimized by the UB3LYP/6311G(d,p)(LANL2DZ) method using the Gaussian 09 AML64-G09 Revision-D.01 program packages (Frisch et al. 2009) and GaussView 6.0.16 (Dennington et al. 2016). Frequency calculations were done to validate vibrational spectra IR by the Opt-Freq keyword (Ramezani et al 2021a, b). The optimized structures, as shown, accurately describe the experimental wavenumbers for free IBgly and its Pt(II) complexes and they are well fitted (Fig. 1 and Table S1 in the supplementary information). Based on these findings, we found that the stretching bands of the asymmetric and symmetric carboxylate groups, as well as the stretching frequencies of the NH and CH groups, are in good agreement with the experimental

Table 1 Molecular Properties of platinum complexes

Compounds	Mw[a] (g/mol) (150–500)	Consensus Log$P_{o/w}$[b] (-2 to 6.5)	TPSA[c] (Å^2) (20 to 130)	No. of ON[d] (< 10)	No. of OHNH[e] (< 5)	Violations of number of rule of 5 (< 5)
IBgly	131.18	**−0.3**	49.33	3	2	0
Complex **1**	359.31	**−1.22**	55.81	5	3	0
Complex **2**	481.43	**1.08**	44.81	5	1	0
Cisplatin	300.05		6.48	2	6	1
Oxaliplatin	397.29	**−0.63**	104.64	4	2	0
Carboplatin	371.25	**−0.63**	59.08	4	2	0

[a]Molecular weight of the molecule

[b]Predicted octanol–water partition coefficient (logP o/w) (–2.0 to 6.5)

[c]Topological polar surface area (PSA) (7.0–200.0)

[d]Number of hydrogen bond acceptors < 10

[e]Number of hydrogen bonds donors < 5

spectra in the theoretical spectra obtained from DFT calculations. This provides additional evidence, that perhaps the optimized structures properly represent the examined molecules and could be used for further theoretical research.

ADME prediction and drug-likeness analysis

The ADME properties of synthesized IBgly ligand and complexes **1** and **2** were predicted using computational research. To determine the brain or gastric absorption of drug, BOILED-EGG presentation can be useful in Swiss ADME well tool (Fig. S14). Figure S14 in supplementary shows ligand; complex **1** and oxaliplatin are in the white section that displays them to be well-absorbed by gastrointestinal organs; while complex **2** and carboplatin are blood–brain barrier (BBB) passively in the yellow part and cisplatin is totally outside the egg. Among them, ligand and carboplatin and complex **1** are red dots and they were read non-substrate and are not actively effluxed by P-glycoprotein$^-$ (PGP$^-$) and other compounds are PGP$^+$ and blue dot. Therefore, we can predict $[Pt(NH_3)_2IBgly]NO_3$ can be a candidate as an oral Pt-drug. The results of the ADME property prediction are shown in Table 1. Qikprop v3.5 (Schrödinger LLC) was used to predict the absorption, distribution, metabolism, and excretion (ADME) properties of all substances. The molecular weight (Mw), predicted octanol–water partition coefficient (log Po/w), number of hydrogen bond acceptors (n-ON), number of hydrogen bond donors (n-OHNH), and topological polar surface area were computed in this study (TPSA). The properties listed above help in determining the ADME qualities of any medication or manufactured molecule. In addition, all compounds demonstrated molecular weight Mw (130–480), ClogP (−0.3 to 1.08), and TPSA (44 to 55) in the acceptable ranges. Interestingly, all synthesized compounds pass the drug-like rules namely Lipinski's rule and Veber's rule (Daina et al. 2017), have desirable drug-likeness criteria. There should be no more than one violation of the following four criteria in a molecule that is likely to be developed as an orally active drug candidate: log Po/w (octanol–water partition coefficient) 5, molecular weight 500, number of hydrogen bond acceptors 10, and number of hydrogen bond donors 5 (Clark and Pickett 2000).

The bioavailability Radar provides drug-likeness of each compound with some factor showing (pink areas) such as lipophilicity (−0.7 to +5.0), size ($150 \leq Mw \leq 500$), polarity (20–130 Å), insolubility ($S \leq 6$), in saturation (amount of sp^3 hybridization of carbon ≥ 0.25), and flexibility (≤ 9) (Daina et al. 2017). Physicochemical aspects of these compounds are displayed in Fig. 2, and it shows all ligand and Pt complexes can be considered as drug candidates like cisplatin, carboplatin, and oxaliplatin. These compounds are acceptably soluble in water. Therefore,

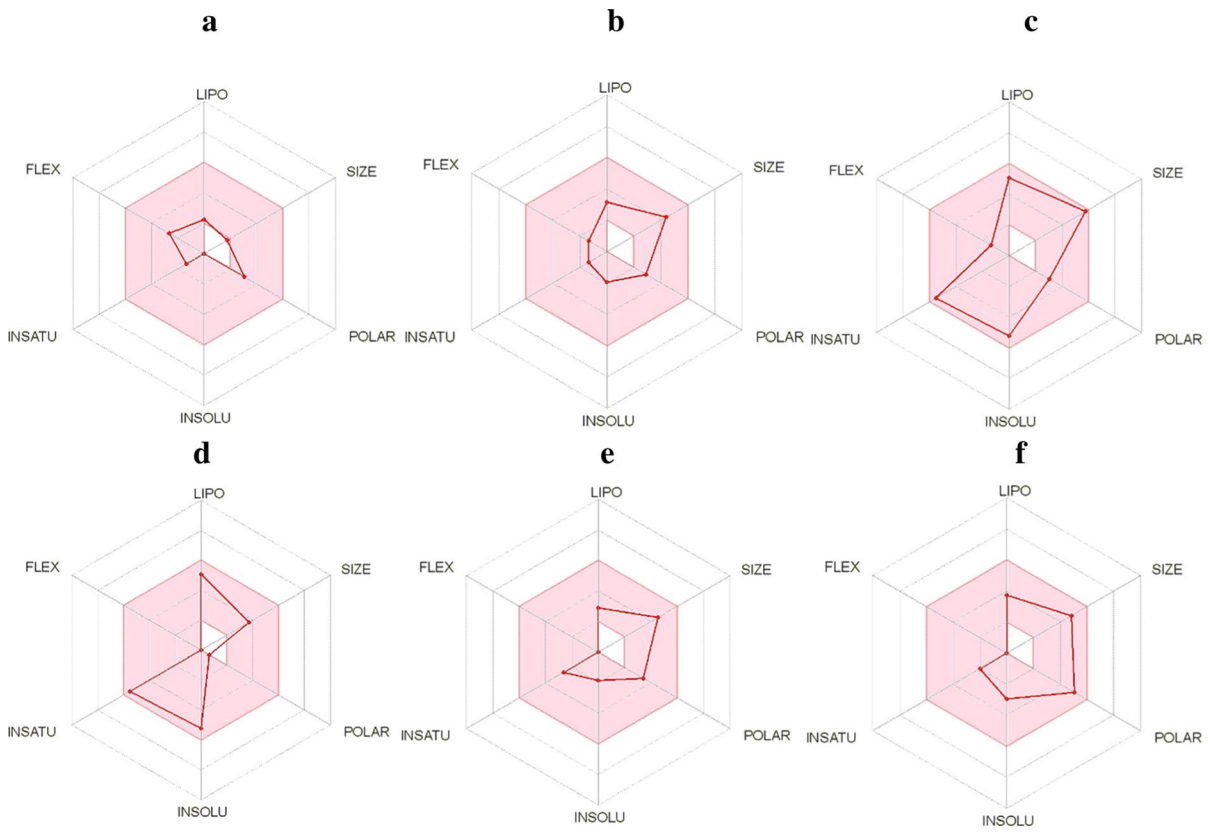

Fig. 2 The bioavailability radar as drug-likeness for **a** IBgly, **b** and **c** complexes **1** and **2**, d-f) cisplatin, oxaliplatin, and carboplatin, respectively

it is good for any designing or formulations as mentioned oral Pt-drug.

DFT investigation

Density functional theory for IBgly and complexes **1** and **2** was applied in the closed-shell singlet ground state to optimize geometries. MEP maps are presented in Fig. 3. The lookout of MEP maps for these compounds demonstrated the O atoms of carboxylate group and N atoms of amino and pyridyl ring can act as donor and acceptor electrons in hydrogen bond and other interactions with DNA. In each molecule, the frontier molecular orbitals are the most significant. Their E_{gen} values and their energy distance (E_{gap}) between LUMO–HOMO indicate their biological activities and the trends in DNA binding affinity (Yadav et al. 2015). The contour plots of HOMO and LUMO for IBgly as a ligand and complexes **1** and **2** as well as their energies are presented in Fig. 4. Negative and positive regions are shown in green and red colors, respectively. HOMO and LUMO calculation of IBgly determine that the surface of HOMO is involved in all orbitals of ligand, and the electron density of LUMO is localized on the amino acid part of IBgly and minimum on the aliphatic branch without considerable contributions. The electron density of HOMO and LUMO for complex **1** is localized mostly on IBgly as well as a metal ion. However, the charge density of HOMO for complex **2** is localized on the chelating ring of IBgly and metal ion, while LUMO is localized on the pyridyl ring of the bipy ligand of the complex. Also, the diagrams of molecular orbitals and energy levels for HOMOs and LUMOs for IBgly and both Pt(II) complexes are presented in Fig. S15 and Table S2 in the supplementary information. For complex **2**, LUMO + n (n = 1–2) was centered on the pyridyl ring of bipy ligand, and HOMO − n (n = 1–2) was populated on carboxylate plus amino groups along with coordinated Pt(II) metal ion. Additionally,

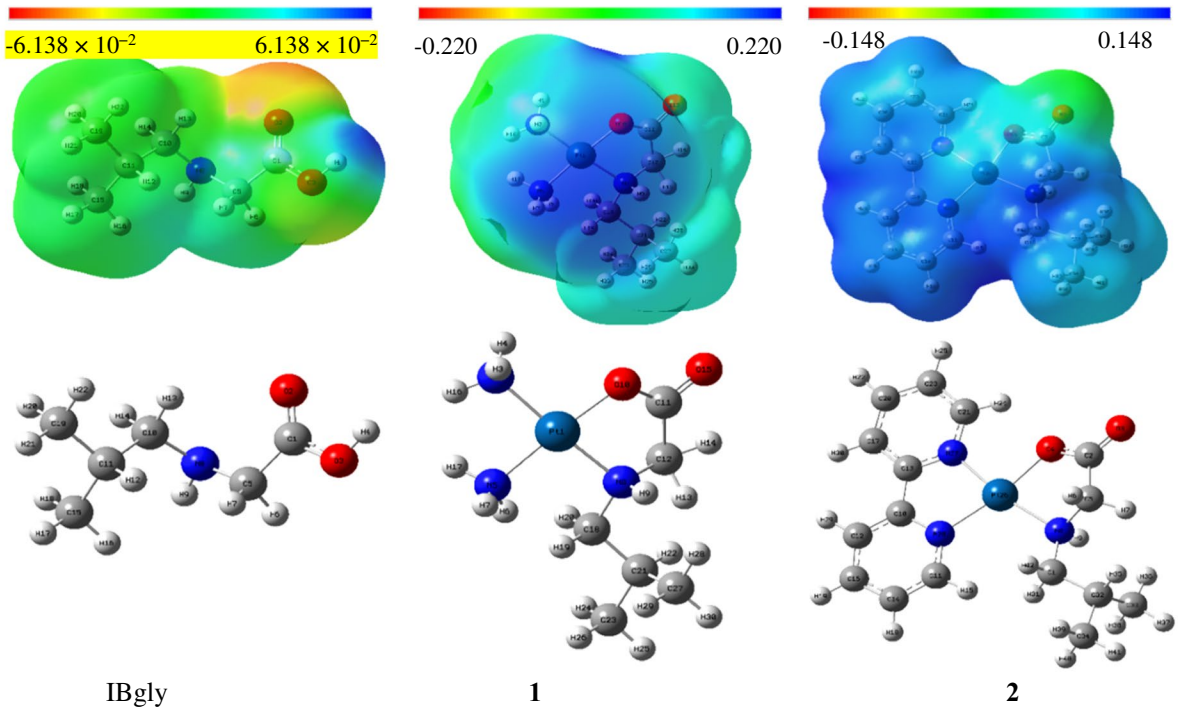

Fig. 3 Optimized structures and MEP maps of IBgly and its Pt(II) complexes **1** and **2**

the calculated quantum chemical parameters of the above-mentioned compounds are calculated and listed in Table 2. Furthermore, many of the theoretical studies have reported that interaction between biomolecules such as DNA or protein and the small molecule can be strong when the E_{HOMO} of the biomolecule is high, while E_{LUMO} of a small molecule is low (Kurita and Kobayashim 2000). The research on the HOMO and HOMO + 1 of DNA has demonstrated that these orbitals are often concentrated on π orbital of base pairs while HOMO + n (n = 2–3) are populated on phosphate backbone (Yadav et al. 2015; Kurita and Kobayashi 2000). In agreement with the above consideration, the intercalation mode is more probably for complex **2**, as the LUMO of complex **2** is localized on the pyridyl ring of bipy. Also, due to HOMO–LUMO orientation of the DNA skeleton and complex **2**, transfer of electronic charge from phosphate groups on DNA to the LUMO of the complex **2** can occur (see Fig. 3). Next, the calculation of the quantum chemical descriptors (QCDs) is an effective technique in determining the activity of molecules. Calculated quantum chemical parameters at the level of theory are listed in Table 2. Among the compounds, the structure of complex **1** has the lowest total Energy (E_{total}) than complex **2** and IBgly. By comparing the E_{gap} between the LUMO and HOMO orbitals of two complexes, we found that the low energy gap of complex **1** can lead to a higher reactivity for this complex with appropriate donors (Yadav et al. 2019). Also, **1** with high values of (σ), is considered as a soft species and more reactive, while for complex **2** is vice versa. On the other hand, complex **2**, with its higher nucleophilicity (N) and chemical potential (CP), will be able to easily deliver its electrons to electrophilic compounds, where electrons can spread throughout the structure.

Natural bond order (NBO) analysis

The atomic charge distributions via natural population analysis (NPA), with UB3LYP/LANL2DZ model, were computed for IBgly and complexes **1** and **2**. For all compounds, the most negative charges of the atomic group were ascribed to nitrogen and oxygen atoms with more electronegativity (Table 3). Specifically, The N8 and O3(IBgly), O10(**1**), O4(**2**) atoms from the chelating ring of amino acid group,

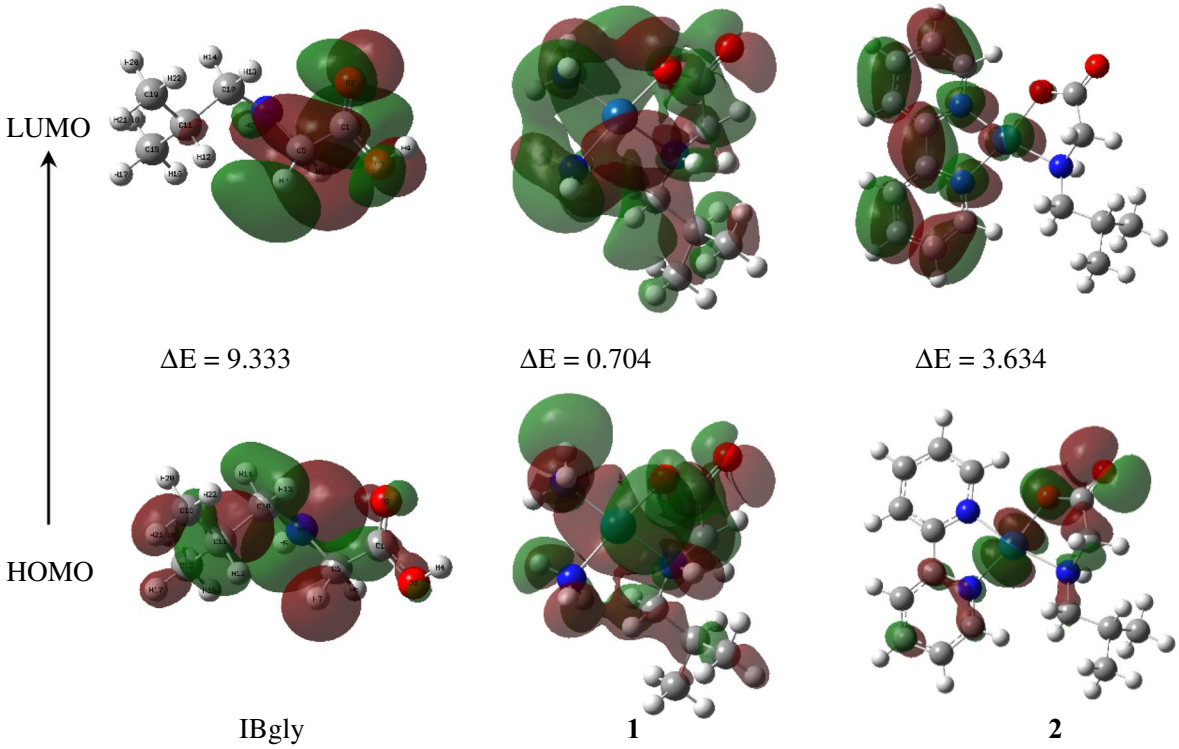

Fig. 4 Contour plots of frontier molecular orbitals with their energy gap (eV) of IBgly and complexes **1** and **2**

Table 2 Calculated quantum chemical parameters of related molecules at the same level of theory

Compound	E_{HOMO}[a]	E_{LUMO}[a]	ΔE_{gap}[a]	η[a]	σ[b]	χ[a]
IBgly	−5.98	3.35	9.33	4.66	0.21	1.31
1	−12.09	−11.39	0.70	0.35	2.84	11.75
2	−9.77	−6.14	3.63	1.82	0.55	7.96
Cisplatin*	−6.618	−1.97	4.47	2.32	0.43	4.29
Compound	CP[a]	ω[a]	N[a]	ΔN_{max}	S[b]	E_{total}[c]
IBgly	−1.31	0.18	5.40	0.28	0.11	−441.67
1	−11.75	196.01	0.01	33.37	1.42	−2337.22
2	−7.96	17.41	0.06	4.38	0.27	−1055.47
Cisplatin	−4.29	3.97	0.25	1.85	0.21	–

[a]In eV, [b] in eV^{-1}, and [c]in Hartree

* These data come from Cohen and Lippard (2001) directly in this column for comparison

and the nitrogen atoms of amino groups and bipyridyl rings of bipy for complexes **1** and **2**, respectively, were susceptible to the electrophilic attack.

Further, the negative charges around Pt atom of N and O atoms were suggestive of electron donation by Pt atom (Table 3). Remarkably, the charges on the N8 (− 0.939 and − 0.773*e*) of the amino group of the chelating ring were more negative than the O atom (− 0.609 and − 0.583*e*) of the carboxyl group for both complexes, respectively. This suggests that the amino

Table 3 Atomic optimized NBO charges of compounds at UB3LYP/LANL2DZ level

Compound Atom	IBgly NBO charges (*e*)	**1** NBO charges(*e*)	**2** NBO charges(*e*)
Pt1(**1**), Pt26(**2**)		+1.071	+0.952
O3(IBgly),O10(**1**), O4(**2**)	−0.571	−0.609	−0.583
N8	−0.538	−0.939	−0.773
N2(**1**), N27(**2**)		−0.995	−0.863
N5(**1**), N28(**2**)		−1.027	−0.823
O2(IBgly),O10(**1**), O4(**2**)	−0.450	−0.464	−0.349
C1(IBgly),C11(**1**), C2(**2**)	+0.584	+0.400	+0.569
H9	+0.302	+0.424	+0.379
H4(IBgly)	+0.409		

Table 4 Bond specification of IBgly compared to its metal complexes from DFT calculations in water

IBgly		**1**		**2**	
Bond lengths (Å)					
C1–O3	1.360	C11–O10	1.434	C2–O4	1.354
C5–N8	1.449	C12–N8	1.511	C5–N8	1.516
C1–O2	1.208	C11–O15	1.258	C2–O3	1.227
C1–C5	1.523	C11–C12	1.603	C2–C5	1.521
N8–H9	1.015	N8–H9	1.000	N8–H9	1.022
		Pt1–O10	1.877	Pt26–O4	2.015
		Pt1–N8	1.974	Pt26–N8	2.145
		Pt1–N2	1.990	Pt26–N27	2.0261
		Pt1–N5	1.990	Pt26–N28	2.081
Bond Angles (°)					
O3–C1–O2	122.60	O10–C11–O15	115.94	O4–C2–O3	123.79
O3–C1–C5	110.06	O10–C11–C12	128.13	O4–C2–C5	113.45
C5–N8–C10	116.81	C12–N8–C18	108.33	C5–N8–C1	112.40
		O10–Pt1–N8	82.85	O4–Pt26–N8	79.49
		O10–Pt1–N2	94.49	O4–Pt26–N27	90.72
		N2–Pt1–N5	89.39	N27–Pt26–N28	79.19
		N5–Pt1–N8	93.28	N28–Pt26–N8	110.61
		N2–Pt1–N8	176.59	N27–Pt26–N8	170.06
		N5–Pt1–O10	176.13	N28–Pt26–O4	169.90

group is more likely to draw the electron density from the Pt center than the carboxyl group. Based on comparing atomic charges in these compounds, it can be stated that the negative charge is accumulated on the N atom the most due to the tendency of the N atom to electrophilic attack and free electron pair on N atoms with negative charges. This is in agreement with the predicted positive charge around the Pt atom (+1.071 and +0.952*e*) for two complexes, respectively. Also, the positive charges of carbon atoms (C11 and C2) of complexes are attributed to the charge donation to the electronegativity oxygen atom from the carboxylate group.

Quantum chemical calculations unmistakably confirmed a square planar geometry for both Pt(II) complexes with appropriate low energy. According to Table 4, O and N atoms of amino acid group coordinated to Pt atom and formed the Pt–N and Pt–O bonds, which causes weakening of the optimized C1–O3 and C5–N8 bond lengths from the free IBgly. These bonds were extended due to coordination with Pt(II) by about 0.1 and 0.02 Å for two complexes,

Table 5 Docking results of complexes with 1BNA

Complex	Rank	Run	$\Delta G°$	$E_{inter\text{-}mol}$[a]	E_{VHD}[b]	E_{elec}[c]	E_{total}[d]	$E_{tortional}$[e]	$RMSD$[f] (A)
IBgly	1	123	−3.69	−5.18	−4.93	−0.25	−1.43	1.49	27.90
1	1	45	−10.44	−11.63	−4.01	−7.62	2.25	1.19	30.31
2	1	62	−9.57	−10.17	−6.71	−3.46	−0.37	0.6	27.68

Energies are given in kcal/mol

[a]Final Intermolecular Energy

[b]Vdw + Hbond + desolve Energy

[c]Electrostatic energy

[d]Final total internal energy

[e]Torsional free energy

[f]Unbound system's energy

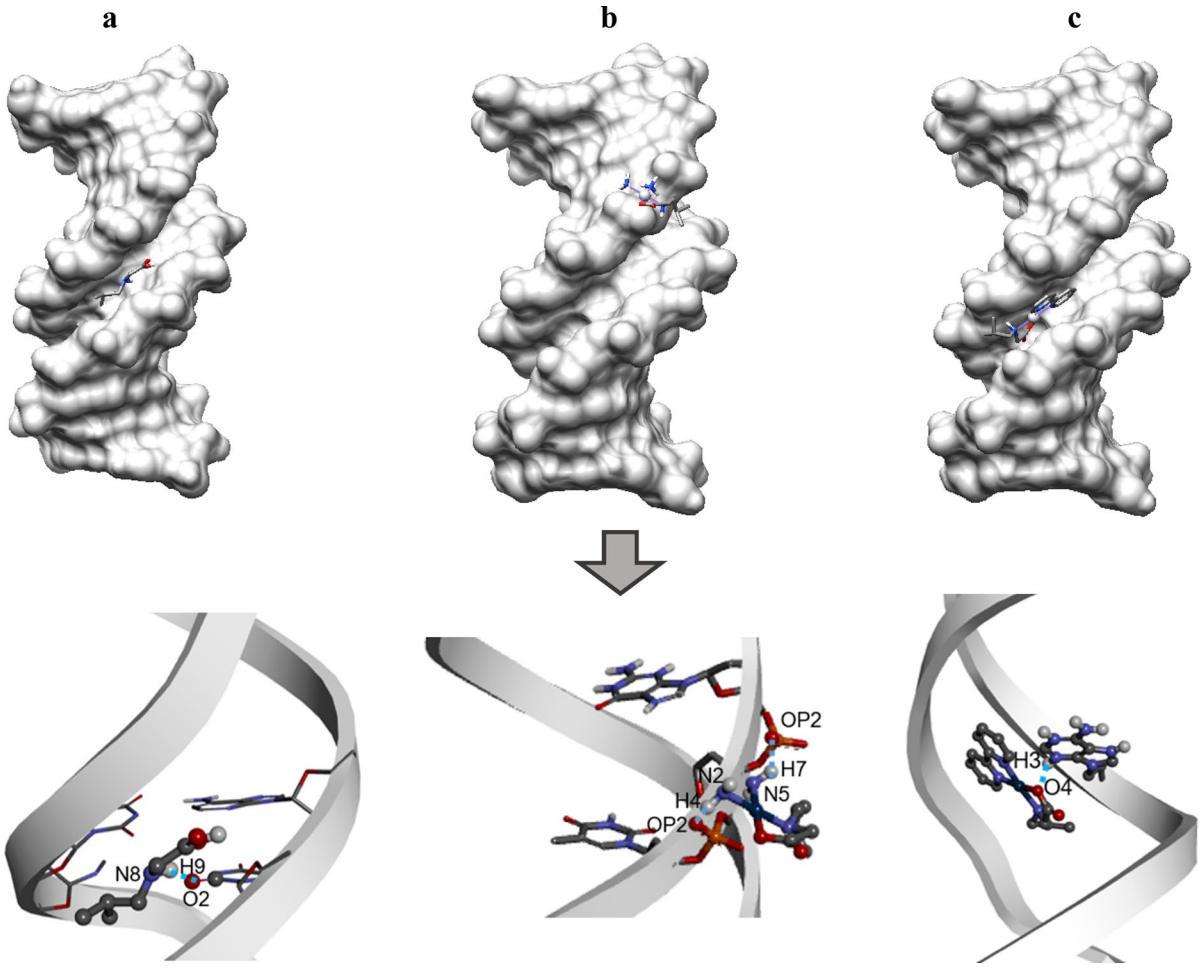

Fig. 5 Computational docking models illustrating the interactions of **a** IBgly and **b** and **c** Pt(II) compounds **1** and **2**, respectively, with 1BNA

respectively. This confirms that the coordination occurs via the N8 and O3 atoms of the amino acid group.

Pt-complex-DNA docking simulation

To understand the interaction of drug-biomolecular, computational molecular docking is an interesting tool while considering structural molecular biology and binding sites on DNA as a target or receptor. This study could be applied to determine the binding and free energies during the investigation of stability and binding mode of drug-receptor complex (Sirajuddin et al. 2013). To this aim, two complexes were docked on B-DNA, which was selected from PDBID: 1BNA. At the beginning of 2000 docking solution was determined for only the lowest relative binding energy in structures docked. Respecting docked structures, two complexes can be well placed into the proper groove of DNA and G–C sites which are stabilized by van der Waals and hydrogen bonding. Specifically, the desolvation, hydrogen bond, and electrostatic energy are effective for approaching complexes to DNA, especially for complex **1** with ammine ligands (−7.62 kcal/mol) + and partially hydrophobic and groove binding type (see Table 5). An optimized docked structure and the hydrogen bonds as (N8–H9···O2(T7); 2.073 Å), (N5–H7···OP2(G22); 2.17 Å and N2–H4···OP2(C21); 1.812 Å), and (A18–H3···O4; 2.106 Å) for IBgly, complexes **1** and **2**, respectively, are shown in Fig. 5. The relative binding energy of the docked structures of IBgly and complexes was obtained −3.69 (IBgly), −11.63 (**1**), and −9.57 (**2**) kcal/mol. The other parameters as both complexes folding energies are presented in Table 5 and Table S3 in the supplementary information.

DNA as a target for complexes

To study the stability of two complexes, at first UV–Vis absorption spectra of complexes **1** and **2** were recorded in double-distilled water solutions (1 mM) at λ_{max} of each complex (Fig. S16), and monitoring was done over time to see any changes (see Fig. S17 in supporting information). DNA is the main target for clinical Pt-drugs in chemotherapy, and electronic absorption monitoring is the most common method to understand the binding and interaction of small drugs with DNA. The sigmoidal isothermal diagrams of DNA denaturation with complexes **1** and **2** represented in Fig. 6 demonstrates increased DNA absorption by titrating each complex. The results of the enhancement in absorption illustrate that the purine and pyrimidine bases have been exposed to ultraviolet light, so platinum complexes are probably able to unzip the two primary strands of DNA

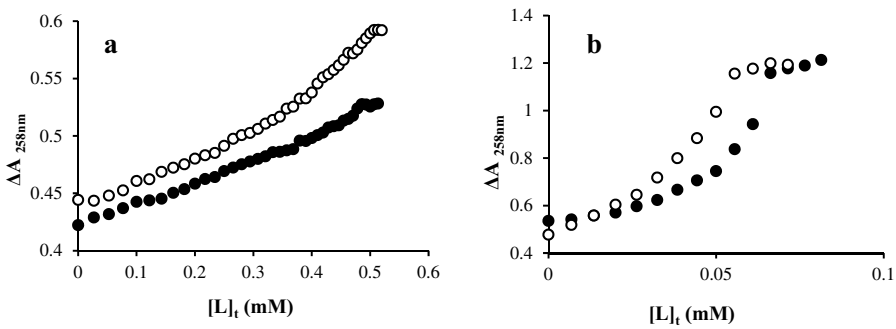

Fig. 6 The DNA denaturation (0.07 mM) by complex titration (0–0.5 mM) of **a** complex **1** and (0–0.1) of **b** complex **2** at 27 (●) and 37 ℃ (●) in Tris–HCl buffer (10 mM sodium chloride, pH 7.4)

Table 6 The thermodynamic values of DNA-Pt complex interactions

Complex	T (℃)	$L_{1/2}$ (mM)	m (kJ mol^{-1}) (mM^{-1})	$\Delta G^{\circ}_{(H_2O)}$ (kJ mol^{-1})	$\Delta H^{\circ}_{(H_2O)}$ (kJ mol^{-1})	$\Delta S^{\circ}_{(H_2O)}$ (kJ mol^{-1} K^{-1})
1	27	0.38	58.6	23.9	231.6	0.69
	37	0.37	40.9	16.9		
2	27	0.04	375.8	16.0	112.4	0.32
	37	0.05	284.1	12.8		

(Greene and Pace 1974). The midpoint concentration of the metal complex during the titration curve ($[L]_{1/2}$) was estimated at 0.379 and 0.368 mM for **1** and 0.038 and 0.055 mM for **2** at 27 and 37 °C, respectively (see Table 6). The low value of $[L]_{1/2}$, especially for complex **2** is ten times smaller than for **1;** thus if being applied as a drug, low doses will be required to interact with this biomacromolecule. The amounts of $[L]_{1/2}$ are approximately the same with values of compounds such as $[Pt(bipy)(But\text{-}gly)]NO_3$ and $[Pt(bipy)(Hex\text{-}gly)]NO_3$ (Eslami Moghadam et al. 2016) and $[Pt(NH_3)_2(amylgly)]NO_3$ (Safa Shams Abyaneh et al. 2018) with CT-DNA. Next, thermodynamic parameters were obtained as summarized in Table 1 using the PACE method and CT-DNA denaturation diagrams (Fig. 6) (Greene and Pace 1974). The values of K and $\Delta G°$ as equilibrium constant and Gibbs free energy of unfolding denaturation, respectively, were computed by Equations $\left(K = \frac{A_N - A_{Obs}}{A_{Obs} - A_D}\right)$ and ($\Delta G° = -RT\text{Ln}K$) for both complexes at 27 and 37 °C (Table 6). The plots of $\Delta G°$ have been drawn *vs* diverse concentrations of complexes **1** and **2** in the transition region at both temperatures (see Fig. S18 in supplementary information). $\Delta G°$ diminished by increasing concentrations for each complex, which is the reason why the interaction process is a spontaneous reaction. A direct line with Equation $\left(\Delta G^{\circ} = \Delta G^{\circ}_{(H_2O)} - m[\text{complex}]\right)$ is obtained from a diagram of $\Delta G°$ versus the concentrations of complexes. The ability of denaturant agent (m), and $\Delta G^{\circ}_{(H_2O)}$ the stability energy of DNA without any denaturant agent is Tabulated in Table 6. According to Table 6, the greater value of m for **2** shows that the denaturation ability of this complex is higher than for **1**. Also, note that the role of temperature as a factor in the denaturation process should be investigated. It can be stated that temperature is one of the influential factors in DNA denaturation because with temperature elevation from 27 to 37 °C, the values of $\Delta G^{\circ}_{(H_2O)}$ for synthesized complexes has been reduced. The next parameter, molar enthalpy of unfolding denaturation by denaturant Pt(II) complexes, within the range of 27–37 °C was computed using Gibbs–Helmholtz equation (Levine 2009). When the values of $\Delta H°$ were schemed *versus* the concentrations of the complexes, descending straight lines were obtained. The molar enthalpy of DNA denaturation in the absence

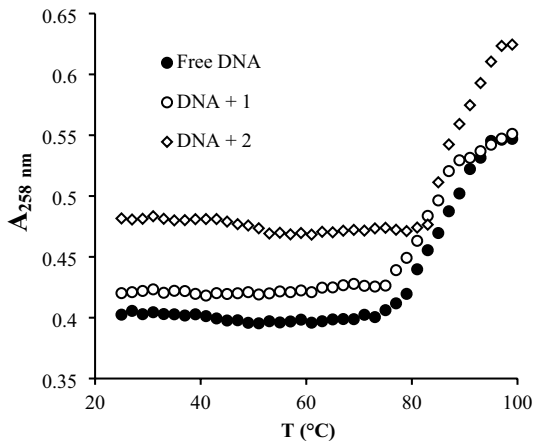

Fig. 7 The diagram of the melting point of free DNA (0.08 mM) and after complexes **1** and **2** addition (0.025 mM) in phosphate buffer

of metal complexes $\Delta H^{\circ}_{(H_2O)}$ was obtained from the interpolation of these lines (see Fig. S19 in supplementary information and Table 1). Ultimately, $\Delta S^{\circ}_{(H_2O)}$ as a molar entropy of DNA unfolding denaturation without any complexes was calculated using Equation $\left(\Delta G^{\circ}_{(H_2O)} = \Delta H^{\circ}_{(H_2O)} - T\Delta S^{\circ}_{(H_2O)}\right)$. The values of $\Delta S^{\circ}_{(H_2O)}$ were positive for DNA denaturation processes by complexes **1** and **2** (Table 6). Data may suggest that the interactions between complexes and DNA contributed to DNA impairment. Indeed, these results show the stability of DNA diminished with complex titration due to a spontaneous and exothermic process. According to a previous report (He et al. 2019), $\Delta H° > 0$ and $\Delta S° > 0$ meant that the hydrophobic interaction is the main force, and $\Delta H° < 0$ and $\Delta S° < 0$ implied that hydrogen bonding and van der Waals forces played the primary role, while $\Delta H° < 0$ and $\Delta S° > 0$ suggested that electrostatic forces were driving the binding. It could be concluded that the complexes with IBgly were maintained by hydrophobic interaction.

In the thermal stability of DNA–complex system, small molecules increase the T_m with binding intercalation mode by about 5–8 °C and increase the Tm slightly with groove binding or electrostatic interactions. Figure 7 displays the curves of absorption changes against temperature rise within the range of 25–99 °C in the absence and presence of complexes

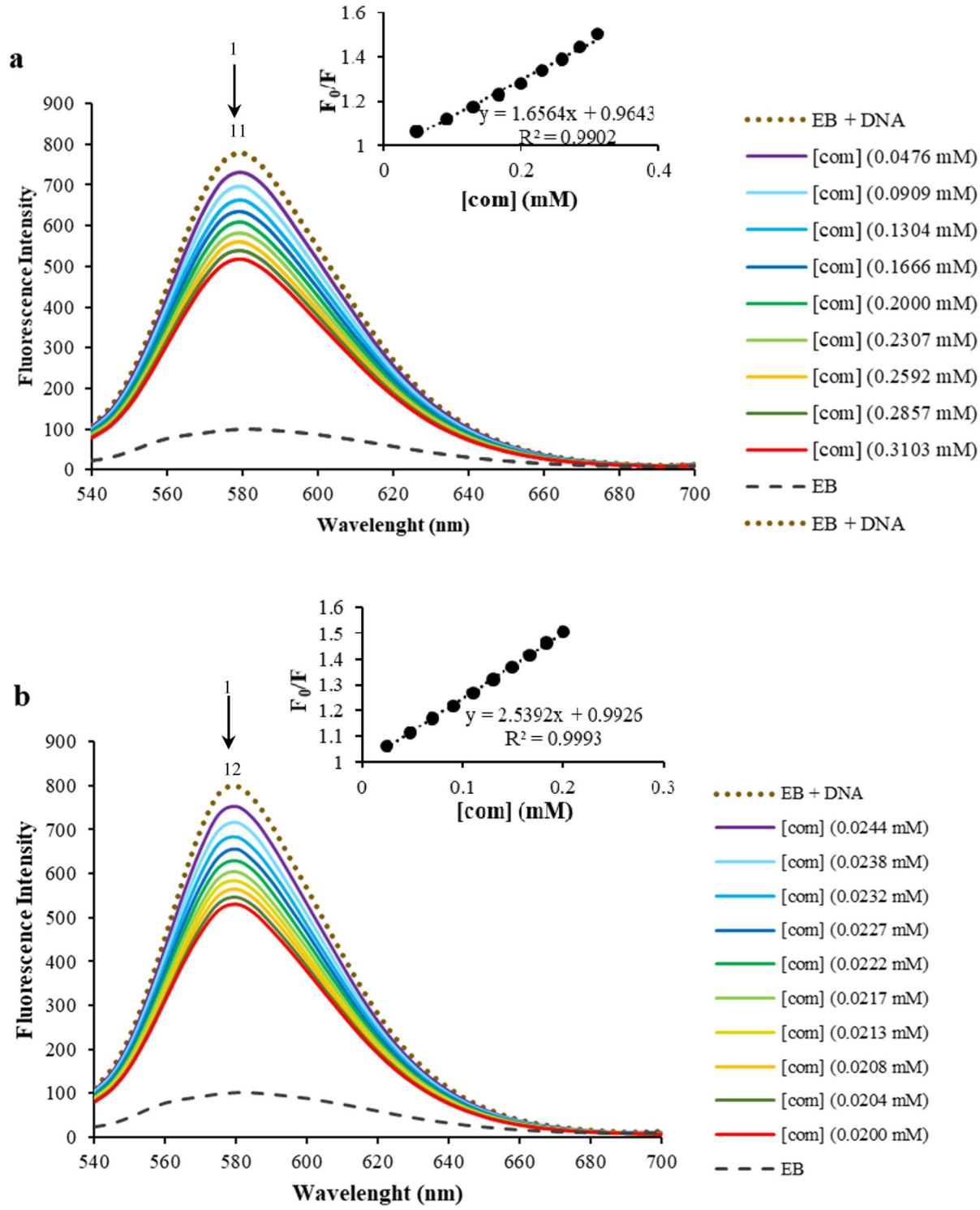

Fig. 8 Change emission of DNA (0.120 mM) and EtBr (0.002 mM) and also complex of **a 1** (0–0.310 mM) and **b 2** (0–0.200 mM) titrating at room temperature. Inset figure: Stern–Volmer plot of Pt complexes in interaction with DNA

Table 7 Calculated fluorescence parameters of synthesized complexes at room temperature

Complex	K_{sv} (M^{-1})	k_q (M^{-1} s^{-1})	R^2	K_b (M^{-1})	n	R^2
1	1.66×10^3	1.66×10^{11}	0.99	3.31×10^3	1.09	0.99
2	2.54×10^3	2.54×10^{11}	0.99	3.77×10^3	1.05	0.99

R is the correlation coefficient

1 and 2. The Tm of DNA in phosphate buffer was reported to be 85 °C in the absence of any additional complexes (Fig. 7). The existence of complexes 1 and 2 changed the Tm values under identical circumstances to 82 and 90 °C, respectively. The findings illustrate why these complexes bonded with CT-DNA as T_m values changed. Complex 2's larger variation in T_m value suggested that it interacted with DNA more, possibly stabilizing the double-strand helix structure than complex 1 via partially groove binding.

The fluorescence emission spectra of EB-DNA as well as after titration by two complexes at 25 °C are presented in Fig. 8. Orderly, fluorescence quenching intensities were reduced without any alteration of maximum emission, which can illustrate the complexes that bind to DNA. According to the Stern–Volmer, Equation ($F_0/F = 1 + K_{sv}[Q] = 1 + k_q\tau_0[Q]$), the quenching mechanism of fluorescence was deliberated (Lakowicz 2006). Where, F_0 and F parameters show the fluorescence intensity of EB-DNA and also after complex titrating **1** and **2** as a quencher, respectively. [Q] denotes the concentration of quencher (Pt(II) complexes). k_q ($k_q = K_{sv}/\tau_0$) shows the biomolecular quenching constant, τ_0 represents the unquenched lifetime of the fluorophore which is around 10^{-8} s, and K_{sv} is the Stern–Volmer

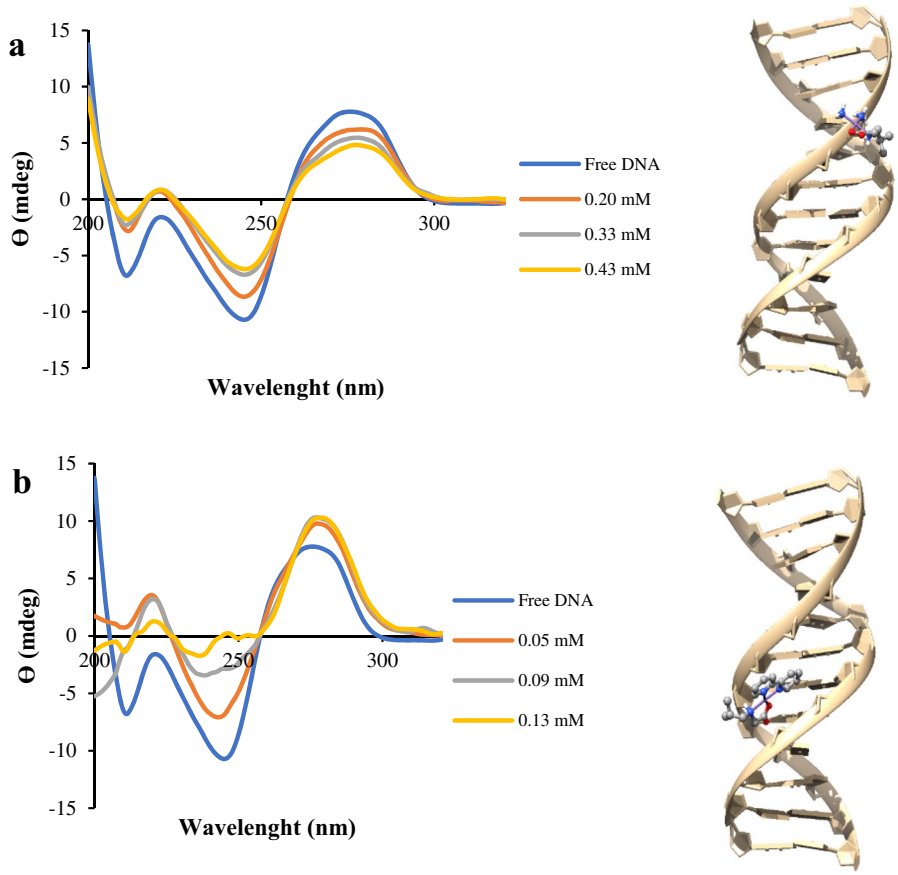

Fig. 9 The ellipticity conformational structure change of free DNA (0.12 mM) at pH 7.4 and 27 ℃ for: **a** and **b 1** (0.2, 0.33 and 0.43 mM) and **2** (0.05, 0.09 and 0.13 mM) complexes, respectively at room temperature

quenching constant acquired from linear F_0/F vs [Q] plot (inset in Fig. 8). The K_{SV} values were calculated to 1.66×10^3 and 2.54×10^3 M^{-1} for **1** and **2**, respectively. The value of K_{SV} for **2** has shown a potential quenching capability, but **1** revealed fewer affinities to DNA binding. It can be evaluated by k_q for detecting the mechanism of quenching containing dynamic or static. The values of k_q for synthesized complexes were greater than those of maximal dynamic quenching constant (2×10^{10} M^{-1} s^{-1}); thus the quenching mechanisms were probably a static quenching for both (Aminzadeh et al. 2020) (see Table 7). The binding data in static quenching system of complexes-DNA at 298 K can be obtained from Equation ($\log(F_0 - F/F) = \log K_b + n\log[Q]$) (Rehman et al. 2015a, b). As shown in $\log F_0/F$ versus $\log[Q]$, the values of K_b and n are defined from the intercept and slope of the line (Fig. S20 in supplementary information and Table 7). The values of K_b for **1** and **2** systems were $3.31–3.77\times10^3$ M^{-1}, respectively, which are lower than the value of K_b for classical intercalators. This is more possible because of approaching via electrostatic force and binding on groove sites via hydrophobic interaction for complexes (Akbay et al. 2009; Husain et al. 2017; Liu and Sadler 2011).

Circular dichroism (CD) of DNA-Pt complexes were shown in Fig. 9, which decreasing negative band intensity originate due to groove binding and other hydrophobic interactions for **1** and **2** (Ramezani et al. 2021a, b; Rehman et al. 2015a, b). Furthermore, the intensity change followed the order **2** > **1**, which was consistent with other spectroscopic methods.

Cytotoxicity data

The anti-proliferative and growth inhibitory activity of two Pt(II) complexes was determined against human model colon cancer cell line HCT116, after 48 and 72 h of incubation. HCT116 cell lines were incubated at 0 to 100 µM of Pt(II) complexes at 37 °C (Fig. 10 and Table 8). The IC_{50} values (50% inhibitory dosage) of each compound were obtained based on the result of Figs. 10 and 11 as well as Table 8. Furthermore, comparison and evaluation of cytotoxicity effects of complexes were investigated with routine chemotherapeutic drugs (cisplatin, carboplatin, and oxaliplatin), which are lower than the IC_{50} amounts of two compounds (see Table 8). Further, based on Fig. 11, for the suppression ability of two compounds, cytotoxic data of each compound were

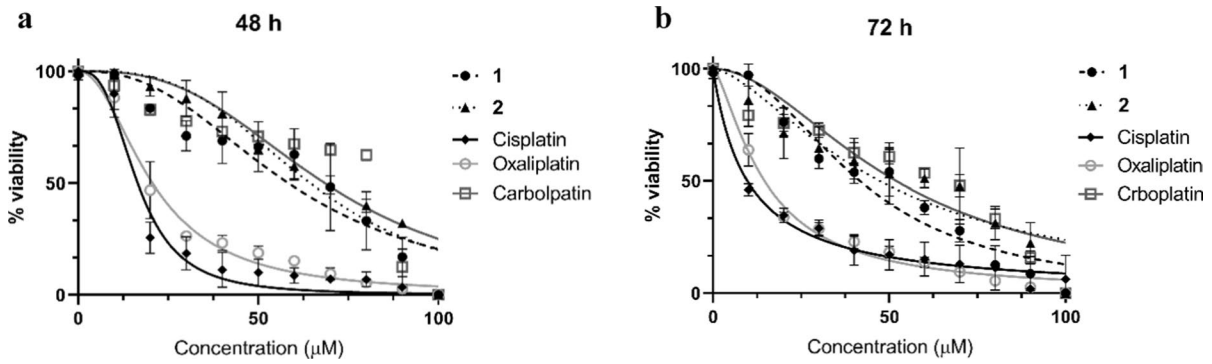

Fig. 10 Inhibition property of Pt-compounds **1**, **2**, (0 to 100 µM) and references drugs against HCT116 cell line incubated after **a** 48 h and **b** 72 h with standard deviation (SD) from at least 3 separate experiments

Table 8 IC_{50} values of Pt-complexes and Pt-drugs against the HCT116 cancer cell line

Complex	IC_{50} (µM) (after 48 h)	IC_{50} (µM) (after 72 h)
$[Pt(NH_3)_2IBgly]NO_3$ (**1**)	58.38 ± 11	41.66 ± 10
$[Pt(bipy)IBgly]NO_3$ (**2**)	64.44 ± 2	47.30 ± 13
Cisplatin	16.56 ± 6	9.72 ± 3
Carboplatin	68.46 ± 1	51.94 ± 1
Oxaliplatin	20.69 ± 2	14.56 ± 2

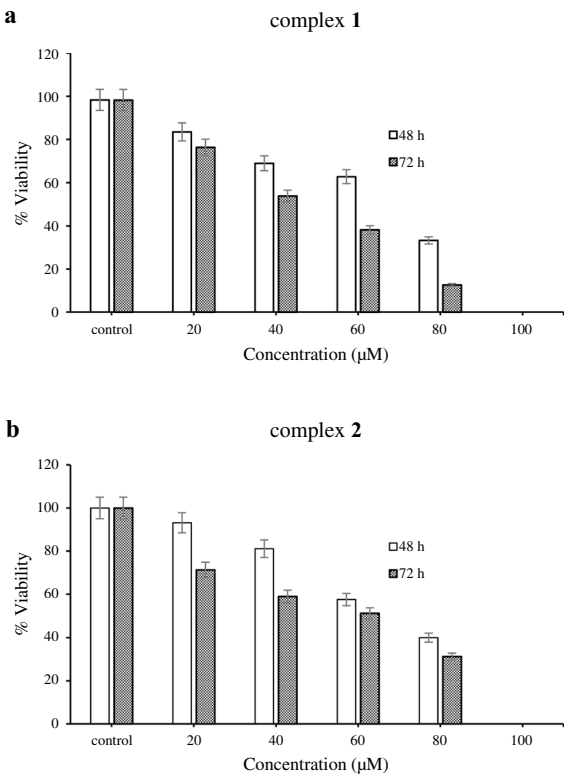

Fig. 11 Bar chart of cell viability percentage of **a** and **b**: complexes **1** and **2** (0 to 100 μM), respectively, on HCT116 cancer cell line after 48- and 72-h incubation. The results are shown as mean ± SD

tabulated and can be compared with each other. On the HCT116 cell line, both complexes showed the IC_{50} values of 58.38 and 64.44 μM in 48 h and 41.66 and 47.30 μM in 72 h incubation times, respectively. Complexes **1** and **2** with the lower IC_{50} values have been more effective on inhibition of colorectal cancer cell line than carboplatin. It was clear that aliphatic glycine as a ligand can play a significant role in cytotoxic property against colorectal cancer cells.

Conclusion

Overall, two complexes $[Pt(NH_3)_2(IBgly)](NO_3)$ (**1**), $[Pt(bipy)(IBgly)](NO_3)$ (**2**), and IBgly as a ligand were synthesized and characterized. Due to good physical properties such as high solubility and stability of these cationic complexes, these compounds could help improve anticancer activity by the presence of leaving group and progressing solubility of them. The IBgly acts as a bidentate ligand via N and O atoms of the amino acid group and forms a 5-membered chelate ring with Pt(II) metal ion. Experimentally, the binding mode of these compounds to DNA was researched using UV–Vis and fluorescence spectroscopy. Thermodynamic and binding parameters for two complexes $\left(\Delta H^{\circ}_{(H_2O)}\right) = 231.6$ and 112.4 kJ mol^{-1} and $\left(\Delta S^{\circ}_{(H_2O)}\right) = 0.69$ and 0.32 kJ mol^{-1} K^{-1}, respectively) indicated that the denaturation of DNA by both complexes occurred as exothermic and spontaneously, but complex **1** had higher potency in DNA denaturation compared with **2**. Moreover, **2** can denature DNA at fewer concentrations than **1**. In the fluorescence study, the quenching mechanism was probably a static quenching for both complexes. Concerning the lower values of K_b for complexes than classical intercalators, it can be expressed these complexes did not bind to DNA from intercalation mode. Spectroscopic studies illustrated that approaching via electrostatic force and groove binding are more possible interactions for both complexes. Aqueous phase theoretical calculations were performed at the UB3LYP level in conjunction with the 6-311G and LANL2DZ basis sets to examine the influence of metal coordination. Also, the DFT studies were used for computing the activity of molecules (QCDs). It was found that complex **1** was more reactive than **2**. Amine derivatives can be considered as an anticancer candidate drug. Further, based on MEP and FMOs, the O atom of the carboxylate group and N atoms of amino and pyridyl ring could act as donor and acceptor electrons in a hydrogen bond. The results of the above were confirmed by DFT and molecular docking studies. Finally, cytotoxic data revealed that both complexes had significant toxicities against the HCT116 cell line after 48 and 72 h of incubation times. In addition, given the values of IC_{50} for both Pt(II) complexes (41.66 and 47.30 μM, respectively), two complexes seemed to have a greater inhibitory effect compared to carboplatin as a commercial drug, in both incubation times 48 and 72 h.

According to ADMET data, complex **1** is projected to be well absorbed by the gastrointestinal tract, but not by the brain or P-gp substrate. However, complex **2** can flow through the BBB and be pumped out of the brain passively. Both Pt complexes are completely pink on the Bioavailability Radar, indicating that

they are drug-like. Positive lipophilicity refers to the fact that complexes **1** and **2** are oral drugs, whereas oxaliplatin, carboplatin, and cisplatin are hydrophilic and injectable. Because all of the complexes were water-soluble, they might be used in the design and formulation of chemotherapeutic drugs. Furthermore, increased bioavailability of the researched complexes was expected when compared to cisplatin, which could indicate that oral formulations of the presented complexes are possible.

Acknowledgements The authors gratefully thank the financial support of this project by the Ferdowsi University of Mashhad, Mashhad, Iran (Grant No. 48899/3) and the Chemistry & Chemical Engineering Research Center of Iran.

Declarations

Conflict of interest The authors declare to have no conflict associated with this work.

References

Akbay N, Seferoğlu Z, Gök E (2009) Fluorescence interaction and determination of calf thymus DNA with two ethidium derivatives. J Fluoresc 19(6):1045–1051. https://doi.org/10.1007/s10895-009-0504-9

Albani JR (2007) Principles and applications of fluorescence spectroscopy. Blackwell Science Publications, Hoboken

Aminzadeh M, Saeidifar M, Mansouri-Torshizi H (2020) Synthesis, characterization, DNA binding, cytotoxicity, and molecular docking approaches of Pd(II) complex with N, O-donor ligands as a novel potent anticancer agent. J Mol Struct 1215:128212. https://doi.org/10.1016/j.molstruc.2020.128212

Bray F, Ferlay J, Soerjomataram I, Siegel RL, Torre LA, Jemal A (2018) Global cancer statistics 2018: GLOBOCAN estimates of incidence and mortality worldwide for 36 cancers in 185 countries. CA Cancer J Clin 68(6):394–424. https://doi.org/10.3322/caac.21492

Castro PM, Jagodzinski PW (1991) FTIR and Raman spectra and structure of $Cu(NO_3)+$ in aqueous solution and acetone. Spectrochim Acta Part A 47(12):1707–1720. https://doi.org/10.1016/0584-8539(91)80008-7

Clark DE, Pickett SD (2000) Computational methods for the prediction of 'drug-likeness.' Drug Discov Today 5(2):49–58. https://doi.org/10.1016/S1359-6446(99)01451-8

Cohen SM, Lippard SJ (2001) Cisplatin: from DNA damage to cancer chemotherapy. Prog Nucleic Acid Res Mol Biol 67:93–103. https://doi.org/10.1016/S0079-6603(01)67026-0

Daina A, Michielin O, Zoete V (2017) SwissADME: a free web tool to evaluate pharmacokinetics, drug-likeness and medicinal chemistry friendliness of small molecules. Sci Rep 7(1):1–3. https://doi.org/10.1038/srep42717

Dennington R, Keith TA, Millam JM (2016) GaussView 6.0. 16. Semichem Inc, Shawnee Mission

Drew HDK, Pinkard FW, Wardlaw W, Cox EG (1932) The structure of the isomeric diamminoplatinous chlorides. Discovery of a third isomeride. J. Chem. Soc., 988-1004 https://doi.org/10.1039/JR9320000988

Eslami Moghadam M, Saidifar M, Divsalar A, Mansouri-Torshizi H, Saboury AA, Farhangian H, Ghadamgahi M (2016) Rich spectroscopic and molecular dynamic studies on the interaction of cytotoxic Pt(II) and Pd(II) complexes of glycine derivatives with calf thymus DNA. J Biomol Struct Dyn 34(1):206–222. https://doi.org/10.1080/07391102.2015.1015056

Fan W, Yung B, Huang P, Chen X (2017) Nanotechnology for multimodal synergistic cancer therapy. Chem Rev 117(22):13566–13638. https://doi.org/10.1021/acs.chemrev.7b00258

Farhangian H, Eslami Moghadam M, Divsalar A, Rahiminezhad A (2017) Anticancer activity of novel amino acid derivative of palladium complex with phendione ligand against of human colon cancer cell line. JBIC J Biol Inorg Chem 22(7):1055–1064. https://doi.org/10.1007/s00775-017-1483-y

Fischer G, Cao X, Cox N, Francis M (2005) The FT-IR spectra of glycine and glycylglycine zwitterions isolated in alkali halide matrices. Chem Phys 313(1–3):39–49. https://doi.org/10.1016/j.chemphys.2004.12.011

Frisch MJ, Trucks GW, Schlegel HB, Scuseria GE, Robb MA, Cheeseman JR et al (2009) Gaussian 09, Revision D.01. Gaussian, Inc, Wallingford

Fugger J, Tien JM, Hunsberger IM (1955) The preparation of substituted hydrazines. I. Alkylhydrazines via alkylsydnones1. J Am Chem Soc 77(7):1843–1848. https://doi.org/10.1021/ja01612a039

Ghalandari B, Poursoleiman A, Fekri M, Komeili A, Divsalar A, Eslami Moghadam M, Kamrava SK, Saboury AA (2019) Biological evaluations of newly-designed Pt(II) and Pd(II) complexes using spectroscopic and molecular docking approaches. J Biomol Struct Dyn 37(13):3422–3433. https://doi.org/10.1080/07391102.2018.1516164

Greene RF, Pace CN (1974) Urea and guanidine hydrochloride denaturation of ribonuclease, lysozyme, α-chymotrypsin, and β-lactoglobulin. J Biol Chem 249(17):5388–5393. https://doi.org/10.1016/S0021-9258(20)79739-5

He C, Liu X, Jiang Z, Geng S, Ma H, Liu B (2019) Interaction mechanism of flavonoids and α-glucosidase: experimental and molecular modelling studies. Foods 8(9):355. https://doi.org/10.3390/foods8090355

Hoffman BL, Schorge JO, Schaffer JI, Halvorson LM, Bradshaw KD, Corton MM (2016) Williams gynecology. The McGraw-Hill education, New York

Hosseinzadeh S, Eslami Moghadam M, Sheshmani S, Shahvelayati AS (2020) Some new anticancer platinum complexes of dithiocarbamate derivatives against human colorectal and pancreatic cell lines. J Biomol Struct Dyn 38(8):2215–2228. https://doi.org/10.1080/07391102.2019.1627909

Husain MA, Ishqi HM, Sarwar T, Rehman SU, Tabish M (2017) Interaction of indomethacin with calf thymus DNA: a multi-spectroscopic, thermodynamic

and molecular modelling approach. MedChemComm 8(6):1283–1296. https://doi.org/10.1039/C7MD00094D

Iakovidis A, Hadjiliadis N (1994) Complex compounds of platinum(II) and (IV) with amino acids, peptides and their derivatives. Coord Chem Rev 135:17–63. https://doi.org/10.1016/0010-8545(94)80064-2

Imaz I, Rubio-Martinez M, An J, Sole-Font I, Rosi NL, Maspoch D (2011) Metal–biomolecule frameworks (MBioFs). Chem Commun 47(26):7287–7302. https://doi.org/10.1039/C1CC11202C

Imran M, Kondratyuk T, Bélanger-Gariepy F (2019) New ternary platinum(II) dithiocarbamates: synthesis, characterization, anticancer, DNA binding and DNA denaturing studies. Inorg Chem Commun 103:12–20. https://doi.org/10.1016/j.inoche.2019.02.007

Kieft JA, Nakamoto K (1967) Infrared spectra of some platinum (II) glycine complexes. J Inorg Nucl Chem 29(10):2561–2568. https://doi.org/10.1016/0022-1902(67)80181-7

Kurita N, Kobayashi K (2000) Density functional MO calculation for stacked DNA base-pairs with backbones. Comput Chem 24(3–4):351–357. https://doi.org/10.1016/S0097-8485(99)00071-6

Lakowicz JR (2006) Principles of fluorescence spectroscopy, 3rd edn. Springer Publications, New York

Latha AA, Anbuchezhiyan M, Kanakam CC, Selvarani K (2017) Synthesis and characterization of γ-glycine—a nonlinear optical single crystal for optoelectronic and photonic applications. Mater Sci 35(1):140–150. https://doi.org/10.1515/msp-2017-0031

Lehninger AL, Nelson DL, Cox MM, Cox MM (2005) Lehninger principles of biochemistry. Macmillan, London

Levine IN (2009) Physical chemistry, 6th edn. McGraw-Hill Education, New York

Liang B, Huo S, Ren Y, Sun S, Cao Z, Shen S (2015) A platinum(IV)-based metallointercalator: synthesis, cytotoxicity, and redox reactions with thiol-containing compounds. Trans Met Chem 40(1):31–37. https://doi.org/10.1007/s11243-014-9886-x

Liu HK, Sadler PJ (2011) Metal complexes as DNA intercalators. Acc Chem Res 44(5):349–359. https://doi.org/10.1021/ar100140e

Liu Y, Tian H, Xu L, Zhou L, Wang J, Xu B, Liu C, Elding LI, Shi T (2019) Investigations of the kinetics and mechanism of reduction of a carboplatin Pt(IV) prodrug by the major small-molecule reductants in human plasma. Int J Mol Sci 20(22):5660. https://doi.org/10.3390/ijms20225660

Mansouri-Torshizi H, Zareian-Jahromi S, Abdi K, Saeidifar M (2019) Nonionic but water soluble, [Glycine–Pd–Alanine] and [Glycine–Pd–Valine] complexes. Their synthesis, characterization, antitumor activities and rich DNA/HSA interaction studies. J Biomol Struct Dyn 37(13):3566–3582. https://doi.org/10.1080/07391102.2018.1520647

Miskowski VM, Houlding VH, Che CM, Wang Y (1993) Electronic spectra and photophysics of platinum(II) complexes with alpha-diimine ligands. Mixed complexes with halide ligands. Inorg Chem 32(11):2518–2524. https://doi.org/10.1021/ic00063a052

Morris GM, Huey R, Lindstrom W, Sanner MF, Belew RK, Goodsell DS, Olson AJ (2019) AutoDock4 and AutoDockTools4: automated docking with selective receptor flexibility. J Comput Chem 30(16):2785–2791. https://doi.org/10.1002/jcc.21256

Nakamoto K (2009) Infrared and Raman spectra of inorganic and coordination compounds part B: applications in coordination, organometallic, and bioinorganic chemistry, 6th edn. Wiley, New York

Oun R, Moussa YE, Wheate NJ (2018) The side effects of platinum-based chemotherapy drugs: a review for chemists. Dalton Trans 47(19):6645–6653. https://doi.org/10.1039/C8DT00838H

Pearson RG (1986) Absolute electronegativity and hardness correlated with molecular orbital theory. Proc Natl Acad Sci USA 83(22):8440–8441. https://doi.org/10.1073/pnas.83.22.8440

Ramezani N, Eslami Moghadam M, Behzad M (2021a) Investigating the anticancer properties of the two new platinum complexes with iso-and tert-pentylglycine by the DFT, molecular docking, and ADMET assessment and experimental confirmations. JBIC J Biol Inorg Chem 26(2):283–298. https://doi.org/10.1007/s00775-021-01851-1

Ramezani N, Eslami Moghadam M, Behzad M, Zolghadri S (2021b) Two new oral candidates as anticancer platinum complexes of 1,3-dimethyl pentyl glycine ligand as doping agents against breast cancer. Spectrochim Acta Part A 251:119415–119428. https://doi.org/10.1016/j.saa.2020.119415

Ramya KS, Iqbal S, Gunasekaran K, Radha A (2018) Anticancer potentials of quassinoids from *Simarouba glauca*–docking and ADME analysis. Res J Life Sci 4(5):218–230

Raudenska M, Balvan J, Fojtu M, Gumulec J, Masarik M (2019) Unexpected therapeutic effects of cisplatin. Metallomics 11(7):1182–1199. https://doi.org/10.1039/c9mt00049f

Rehman SU, Sarwar T, Husain MA, Ishqi HM, Tabish M (2015a) Studying non-covalent drug–DNA interactions. Arch Biochem Biophys 576:49–60. https://doi.org/10.1016/j.abb.2015.03.024

Rehman SU, Sarwar T, Ishqi HM, Husain MA, Hasan Z, Tabish M (2015b) Deciphering the interactions between chlorambucil and calf thymus DNA: a multi-spectroscopic and molecular docking study. Arch Biochem Biophys 566:7–14. https://doi.org/10.1016/j.abb.2014.12.013

Rosado MT, Duarte ML, Fausto R (1998) Vibrational spectra of acid and alkaline glycine salts. Vibrat Spec 16(1):35–54. https://doi.org/10.1016/S0924-2031(97)00050-7

Rozencweig M, Von Hoff DD, Slavik M, Muggia FM (1977) Cis-diamminedichloroplatinum(II): a new anticancer drug. Ann Intern Med 86(6):803–812. https://doi.org/10.7326/0003-4819-86-6-803

Safa Shams Abyaneh F, Eslami Moghadam M, Hossaini Sadr M, Divsalar A (2018) Effect of lipophilicity of amylamine and amylglycine ligands on biological activity of new anticancer cisplatin analog. J Biomol Struct Dyn 36(4):893–905. https://doi.org/10.1080/07391102.2017.1301273

Sirajuddin M, Ali S, Badshah A (2013) Drug–DNA interactions and their study by UV–Visible, fluorescence spectroscopies and cyclic voltametry. J Photochem Photobiol B 124:1–19. https://doi.org/10.1016/j.jphotobiol.2013.03.013

Wani TA, Alsaif N, Bakheit AH, Zargar S, Al-Mehizia AA, Khan AA (2020) Interaction of an abiraterone with calf thymus DNA: investigation with spectroscopic technique and modelling studies. Bioorg Chem 100:103957. https://doi.org/10.1016/j.bioorg.2020.103957

Wilson JJ, Lippard SJ (2014) Synthetic methods for the preparation of platinum anticancer complexes. Chem Rev 114(8):4470–4495. https://doi.org/10.1021/cr4004314

Wiltshaw E (1979) Cisplatin in the treatment of cancer. Platin Met Rev 23(3):90–98

Xu ZH, Chen FJ, Xi PX, Liu XH, Zeng ZZ (2008) Synthesis, characterization, and DNA-binding properties of the cobalt(II) and nickel(II) complexes with salicylaldehyde 2-phenylquinoline-4-carboylhydrazone. J Photochem Photobiol A 196(1):77–83. https://doi.org/10.1016/j.jphotochem.2007.11.017

Yadav S, Yousuf I, Usman M, Ahmad M, Arjmand F, Tabassum S (2015) Synthesis and spectroscopic characterization of diorganotin(IV) complexes of N′-(4-hydroxypent-3-en-2-ylidene) isonicotinohydrazide: chemotherapeutic potential validation by in vitro interaction studies with DNA/HSA, DFT, molecular docking and cytotoxic activity. RSC Adv 5(63):50673–50690. https://doi.org/10.1039/C5RA06953J

Yadav P, Yadav JK, Agarwal A, Awasthi SK (2019) Insights into the interaction of potent antimicrobial chalcone triazole analogs with human serum albumin: spectroscopy and molecular docking approaches. RSC Adv 9(55):31969–31978. https://doi.org/10.1039/C9RA04192C

Zhao N, Yan L, Zhao X, Chen X, Li A, Zheng D, Zhou X, Dai X, Xu FJ (2018) Versatile types of organic/inorganic nanohybrids: from strategic design to biomedical applications. Chem Rev 119(3):1666–1762. https://doi.org/10.1021/acs.chemrev.8b00401